

Radar Application to Monitoring of Fluid Migration in Porous Material

著者	金 東勲
学位授与機関	Tohoku University
URL	http://hdl.handle.net/10097/50273

Radar Application to Monitoring of Fluid Migration in Porous Material

レーダを利用した空隙を持つ
物質中の液体移動モニタリング

by
Dong-Hun Kim

Submitted to Tohoku University

for
Master of Environmental Studies

Committee in charge:
Prof. Motoyuki Sato, Tohoku Univ.
Prof. Takatoshi Ito, Tohoku Univ.
Assoc. Prof. Yuichi Niibori, Tohoku Univ.

February, 2011

Contents

Chapter 1 Introduction

1.1 Background of the research	1
1.2 Contents of dissertation	7

Chapter 2 Principles of fluid migration in porous material

2.1 Fluid migration in unconsolidated sand	8
2.2 Subsurface water migration	10

Chapter 3 Configuration of GPR Measurements

3.1 Measurement of fluid migration	12
3.1.1 Characteristics of the host material	12
3.1.2 Characteristics of fracture fluid	13
3.1.3 Method of hydraulic fracturing	14
3.1.4 Measurement system configuration	15
3.1.5 Vivaldi array antenna	16
3.2 Measurement of water migration in Vadose zone	19
3.2.1 Characteristics of Vadose zone	19
3.2.2 Characteristics of migrated water	19
3.2.3 Method of water injection	22
3.2.4 Measurement system configuration	22
3.2.5 Dipole array antenna	22
3.2.6 Optical link system	24
3.2.7 Evaluation of measurement system	25

Chapter 4 Experiments

4.1 Monitoring of fluid migration in a sand specimen	27
4.1.1 Experiment results	28
4.1.2 Frequency shift analysis	37
4.2 Monitoring of the subsurface water migration by borehole radar	40

4.2.1 Experiment results	41
4.2.2 Analysis	46
Chapter 5 Fluid Migration Modeling	
5.1 Modeling of the fluid migration in a sand specimen	49
5.1.1 1-D (Dimensional) model	49
5.1.2 3-D model	51
5.1.3 Analysis	54
5.2 Modeling of the subsurface water migration	54
5.2.1 Piston model without edge leakage effect	54
5.2.2 Piston model with edge leakage effect	56
Chapter 6 Conclusions	58
Appendix	
A.1 Volumetric moisture contents in the condensed region	61
A.2 2-D tomography	61
References	65
Publications	67
Acknowledgement	68

List of figures

Chapter 1 Introduction

Fig. 1.1 Hydraulic fracturing for extraction of methane hydrate.	3
Fig. 1.2 Performance of surface-based GPR with survey region.	5
Fig. 1.3 Performance with survey region of (a) single-hole radar (b) cross-hole radar.	6
Fig. 1.4 Nuclear waste disposal facility.	6
Fig. 1.5 SPR storage.	7

Chapter 2 Principles of fluid migration in porous material

Fig. 2.1 Methane hydrate phases.	9
Fig. 2.2 Cross-section of specimen.	10

Chapter 3 Configuration of GPR Measurements

Fig. 3.1 Waveform of received signal.	13
Fig. 3.2 Fracturing fluid in a box to acquire its electric permittivity.	14
Fig. 3.3 Test specimen for hydraulic fracturing.	15
Fig. 3.4 Observation result of pulse generator signal.	16
Fig. 3.5 Vivaldi antenna element (a) Front side (b) Back side, Vivaldi array antenna (c) Front side (d) Back side, Unit = mm.	17
Fig. 3.6 Return losses of Vivaldi antenna element and Vivaldi array antenna (a) Measurement (b) Simulation.	18
Fig. 3.7 Radiation patterns of Vivaldi antenna element and Vivaldi array antenna at 3 GHz (a) H-plane (Measurement) (b) E-plane (Measurement) (c) H-plane (Simulation) (d) E-plane (Simulation).	18
Fig. 3.8 Borehole radar experiment (a) A complete view (b) Measurement instruments (c) Antennas (d) System diagram.	21
Fig. 3.9 Appearance of dipole antennas (a) Cylindrical dipole antenna (b) Rod-type dipole antenna.	23
Fig. 3.10 Return loss of dipole antennas.	24
Fig. 3.11 Radiation pattern of a dipole antenna (E-plane) (a) Cylindrical dipole antenna (b) Rod-type dipole antenna.	24
Fig. 3.12 Optical link system (a) Down link (Antenna) (b) An optical probe.	25

Fig. 3.13 Power spectrum of optical link system with attenuation (a) Optical down link (b) Optical probe.	25
Fig. 3.14 Transmission between dipole antennas.	26

Chapter 4 Experiments

Fig. 4.1 Inner structure of specimen.	28
Fig. 4.2 Configuration of measurement system.	29
Fig. 4.3 Pressure of mixed fracturing fluid.	30
Fig. 4.4 Cross-section of specimen.	30
Fig. 4.5 Schematic diagrams of propagating wave paths which have a distance (a) 11 cm (b) 11.40 cm (c) 12.53 cm (d) 14.21 cm.	31
Fig. 4.6 Travel times to propagating wave paths which have a distance (a) 11 cm (b) 11.40 cm (c) 12.53 cm (d) 14.21 cm.	32
Fig. 4.7 Arrival time of the infiltrated region.	33
Fig. 4.8 Pressure of mixed fracturing fluid.	34
Fig. 4.9 Cross-section of specimen.	35
Fig. 4.10 Schematic diagrams of propagating wave paths which have a distance (a) 11 cm (b) 11.40 cm (c) 12.53 cm (d) 14.21 cm.	35
Fig. 4.11 Travel times to propagating wave paths which have a distance (a) 11 cm (b) 11.40 cm (c) 12.53 cm (d) 14.21 cm.	37
Fig. 4.12 Arrival time of the infiltrated region.	37
Fig. 4.13 Residual spectral centroid (a) Example for explanation a concept of residual spectral centroid (b) Residual spectral centroid (c) Effective bandwidth.	40
Fig. 4.14 Setup of borehole radar.	41
Fig. 4.15 Travel times by first peak and leading edge.	42
Fig. 4.16 1 st experiment time domain analysis (a) Travel time (b) Apparent permittivity	44
Fig. 4.17 1 st experiment residual variation at 225 MHz.	44
Fig. 4.18 2 nd experiment time domain analysis (a) Travel time (b) Apparent permittivity	46
Fig. 4.19 2 nd experiment residual variation at 225 MHz.	46
Fig. 4.20 Differential permittivity profile with time.	47
Fig. 4.21 Variation of travel times with water infiltration.	48

Chapter 5 Fluid Migration Modeling

Fig. 5.1 1-D (Dimensional) model (a) 1-D (Dimensional) migration model (b) Travel time with $\epsilon_{r,II}$.	50
Fig. 5.2 3-D (Dimensional) model (a) Hypothesis I (b) Hypothesis II and III.	52

Fig. 5.3 FDTD results (a) Hypothesis I (b) Hypothesis II (c) Hypothesis III.	53
Fig. 5.4 Effect of water front movement to travel time.	55
Fig. 5.5 Normalized fluctuation of electric permittivity.	55
Fig. 5.6 Envelop infiltration velocity and water front depth.	57

Appendix

Fig. A.1 2-D electric permittivity tomography (a) Mapping (b) Initial (0 min) (c) After breakdown (3 min) (d) Final (15 min).	64
---	----

List of tables

Chapter 2 Principles of fluid migration in porous material

Table 2.1 Saturated hydraulic conductivity (K) values found in nature.	11
--	----

Chapter 4 Monitoring of Fluid Migration in Specimen and Subsurface

Table 4.1 Specifications of measurement.	28
Table 4.2 Specifications of measurement.	40
Table 4.3 Zero-distance delay times.	43
Table 4.4 Arrival time of the infiltrated water.	43

Chapter 5 Fluid Migration Modeling

Table 5.1 Mean and variance values of infiltration velocity.	56
Table 5.2 Mean and variance values of infiltration velocity.	56

Chapter 1

Introduction

1.1 Background of the research

Radar application to monitoring of fluid migration in porous material

With the advancement of civilization, environmental monitoring has been developed and conducted to overcome natural disasters and acquire useful resources. In the lower level of civilization, people had prepared catastrophes and detected essential materials using primitive human senses and experiences like an eyesight, a hearing, and a simple statistics. However, measurement methods have been improved drastically with a progress of science since the industrial revolution. One of them is a radar measurement for environmental monitoring. Radar is an abbreviation word of “radio detection and ranging”, it means that radar was basically developed for detecting and ranging of target using electromagnetic waves. Radar was required to not only discriminate a target signal from a clutter signal but also estimate a size, a shape, and a material of target, because it is worked means of surveillance and reconnaissance for military purpose. After World War II ended, many advanced military technologies were transferred from exclusive defense research institutions and industries to civilian sectors. Radar was applied abilities of detecting and ranging to air traffic control, ship navigator, and altimeter. Environmental monitoring was also adapted radar for one of remote sensing methods.

In the preparation for preventing natural disasters, traditional environmental monitoring methods were sensed variations of circumstance directly by naked eyes and other senses. Thus observation range is restricted within short limits and observation accuracy is poor. However radar is observed indirectly using electromagnetic waves, observation range and accuracy are drastically increased. For instance, movement of clouds which is important to weather forecast is detected only line of sight by naked eyes. However radar can detect clouds theoretically almost 360 km distance between a cloud and a ground station, and even estimate volume and density of clouds which is measured by Doppler effect and reflectivity of electromagnetic waves. On the other hand, SAR (Synthetic Aperture Radar) is worked for environmental monitoring of the earth surface in the aerospace. Electromagnetic waves can penetrate obstacles like clouds in the troposphere, however visible ray used for optical methods is difficult to do that. Because visible ray has more high frequency than electromagnetic waves, thus its attenuation in vapor is also relatively large. SAR can provide target information like a position, an altitude, and a polarimetric characteristic. Those things help to set countermeasures deal with calamities.

In the growth of population and the improvement of living, resources demand is also increased. It

leads to diminish R/P (Reserve/Production) ratio, we must prepare a resource crisis. A fundamental solution is a development of new substitute resources which are enhanced the efficiency and the convenience. However it takes a lot time and cost for research and practical use. Thus a realistic solution is an increasing reserve of resources by advanced surveillance technologies. One of them is GPR (Ground Penetrating Radar) which is geophysical and un-destructive method. It is worked in the subsurface that is different to general radar working place. GPR is adopted various techniques from other fields, because the subsurface consists of inhomogeneous and dispersive materials.

This thesis is focused on system design, measurement, and signal analysis for environmental monitoring by two different types of GPR.

Preliminary experiments of the hydraulic fracturing for enhancing extraction techniques of the methane hydrate

Most variation of strata structure in the subsurface is difficult to observe directly, thus we can only estimate phenomenon using data acquired by several remote sensing methods. However that analysis is based on physical approximations and hypotheses, sometimes it makes fatal errors in the realistic situation. When we establish a theory about the geology scientifically, obvious evidences must be presented. For example, numerical indicators like pressure and temperature, and remain traces like fracture and metamorphosis caused by variation of numerical indicators. However it is spent a lot of time and cost to excavating or boring, thus we conduct preliminary experiments using down-scaled specimens in the laboratory [1].

Methane hydrate is one of leading substances to substitute existing fossil fuels. Although people mentioned several alternative energies which are photovoltaics, wind and geothermal energies, and nuclear fusion power, there are critical weakness points to use general purpose. Operation time of photovoltaics, wind and geothermal energies are restricted by regional climate conditions and the topography. In the mobility and the storage of energy, photovoltaics are depended on electric and electronic devices like battery and regulator. Nuclear fusion power is required several revolutionary technologies to solve stabilization of fusion state which is under high temperature and pressure conditions. Expected accomplishment date of these technologies for commercial usage is at least 2050s. Consider our energy consumption and expected expire date of conventional energy sources, we cannot wait until 2050s. In these reasons, the development of the methane hydrate is being watched with keen interest.

Conventional extraction method has applied a spurt generated by spontaneous or artificial tectonic stresses. However extraction of the methane hydrate is relatively more difficult than conventional extraction for petroleum and natural gas, because methane hydrate reserved as solid form in the subsurface. Thus we must transform solid state of methane hydrate into liquid or gas states of methane hydrate using depressurization, thermal stimulation, and possibly solvent injection [2]. These methods

are required fractures in the subsurface to infiltrate decrease of pressure, heat, or solvent. In the production of methane hydrate, there are two roles of borehole. One is the injection borehole used a path of pressure, heat or solvent. Another is the production borehole used a path of dissolved or evaporated methane hydrate. Generally extraction methods for methane hydrate production are required artificial fractures to connect boreholes. Artificial fracture is also related the methane hydrate production. Hydraulic fracturing is commonly used to develop fracture in the energy extraction and the manufacture applications as shown in Fig.1.1. Principle of hydraulic fracturing in the consolidated rock which is tightly bound geologic formation composed of sandstone, limestone, granite, or other rock is well explained as a theory. On the other hands, there is no apparent an explanation about hydraulic fracturing of the unconsolidated rock that appears in the form of loose particles. It is difficult to increase methane hydrate extraction efficiency, because most methane hydrate reservoirs exist under the sea-bed which consists of unconsolidated rocks.

There are several geophysical measurement methods for geological investigation. However verification of measurement result is difficult, because we cannot access to geological site directly. For this reason, preliminary experiments using down-scaled specimens of the unconsolidated rock are conducted. The measurement result of hydraulic fracturing process in the specimen will be applied to enhance the extraction techniques of the methane hydrate.

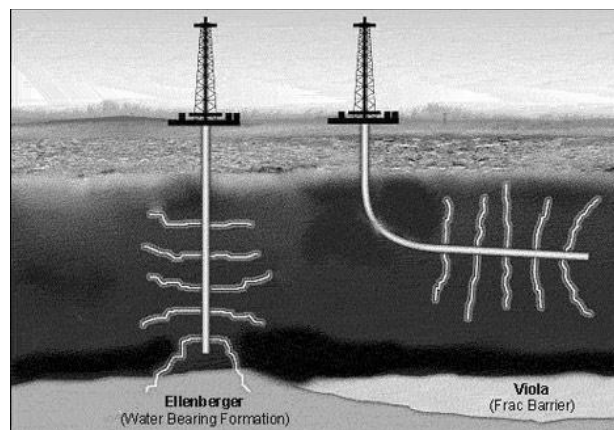


Fig.1.1 Hydraulic fracturing for extraction of methane hydrate.

(<http://wastedenergy.net/2010/05/07/poofy-poofy/>)

Borehole radar for monitoring of the subsurface water migration

Borehole radar is one of GPR methods to investigate deep subsurface circumstance especially. Surface-based GPR methods move transmitting and receiving antennas on the surface as shown as Fig.1.2, and express the 2-D or 3-D subsurface circumstance by signal and image processing. In this time, received signal consists of reflected wave generated from target, clutter, and surface. Even antennas mutual coupling called as direct wave also affects received signal. In view of an investigating area, surface-based GPR covers several types of land surface which is possible antenna

to contact to surface. Detecting range of surface-based GPR methods from surface to subsurface is restricted few meters by homogeneity and attenuation of subsurface circumstance and antenna characteristics and formation. On the other hand, antennas of borehole radar are inserted into tens or hundreds meters borehole. Detecting range of borehole radar from surface to subsurface is depended on a borehole length. Thus borehole radar has an advantage of deep subsurface investigation. There are two antenna insertion types of borehole radar. One is called as single-hole radar which transmitting and receiving antennas are inserted into single borehole as shown in Fig.1.3(a). Another is called as cross-hole radar which transmitting and receiving antennas are inserted into different boreholes respectively as shown in Fig.1.3(b). Detection coverage of single-hole radar is expressed as a cylinder, because dipole or cylindrical slot antennas commonly used for borehole radar have an omnidirectional radiation pattern. It means that received signal consists of reflected waves from different directions. Solving this problem, directional borehole radar which receiving antenna is adopted array structure to discriminate phase difference generated by distance from target to each array elements is devised [3]. On the other hand, detection coverage of cross-hole radar is a cross-section between Tx antenna inserted borehole and Rx antenna inserted borehole as shown in Fig.1.3(b). It indicates that received signal consists of transmitted waves penetrated through transmission media between Tx and Rx antennas. Cross-hole radar has relatively small detection coverage, however it is the same meaning that received signal is less affected by reflected waves from clutters. And analysis of transmitted wave has more advantage to discriminate characteristics of a target, for instance a cavity filled with air or water, a dielectric material, and a conductor.

Monitoring of subsurface water around cellarage like nuclear waste disposal facility and SPR (Strategy Petroleum Reserve) storage is important to avoid environmental contamination and reduction of facility durability. Nuclear waste is discriminated three types by intensity of radioactivity. High level radioactive wastes like depleted nuclear fuel rod can be reprocessed. However it takes a lot of cost and only a few Uranium 235 is collected for nuclear fuel. Even a byproduct of reprocessing, Plutonium 239 is difficult to use a nuclear fuel and can be diverted to nuclear weapon. For this reason, reprocessing is restricted and controlled by IAEA (International Atomic Energy Agency). Most countries running nuclear power plants, high level radioactive wastes are kept in the cellarage semi-permanently. We know about a nightmare of Chernobyl nuclear power plant accident, these wastes should be isolated from our lebensraum immediately. Middle and low level nuclear wastes produced during operation of nuclear power plants are also required to isolate. These nuclear wastes are mixed with concrete and contained in stainless steel drums, then stored in the nuclear waste disposal facility as shown in Fig.1.4. Solidified nuclear wastes are difficult to leak from the nuclear waste disposal facility. Because the facility is surrounded by impermeable strata, subsurface water is hard to infiltrate into the facility and exude from the facility. It is also applied SPR storage to do same. SPR storage is discriminated two types by a place of storage. One is a ground-tank which has advantages to the

construction term and simplicity. However it has disadvantages to the safety, a cost of construction and maintenance, a natural attenuation. For this reason, massive SPR storage (\geq Mbbl) is used to a salt cavern (or dome) or a constructed cavern. These caverns are connected to the ground by cargo-shipment pipe, thus a pressure of the inner cavern is lower than a tectonic stress of the circumference. For this reason, cavern is damaged and cracked by a geological process, reserved crude oil or petroleum products are difficult to evade from the cavern. Even subsurface water infiltrates into the cavern and works like oil-proof agent.

There are several requirements to select a site of nuclear waste disposal facility and SPR storage. For example, not only economical factors like accessibility to a port of shipment and a major consumption region but also safety factors like stability of bedrock and existence of earthquake and fault zone, even regional arrangement. Geophysical methods are applied to investigation related with safety factors. Especially, borehole radar is available to long-term survey of subsurface water system around site, because other geophysical methods are difficult to detect variation of subsurface water distribution. Radioactive methods can survey a flow network, however tracer used to track the localization of a specific compound affects the subsurface environment.

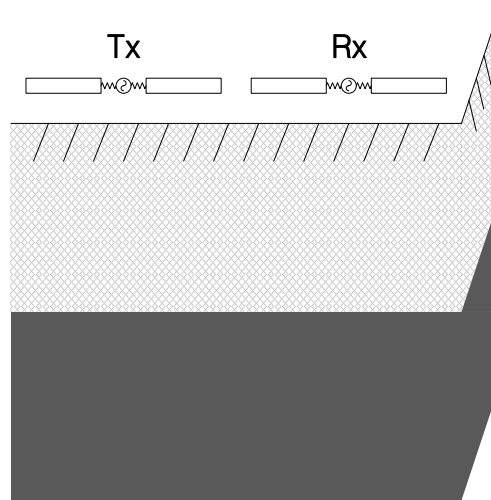


Fig.1.2 Performance of surface-based GPR with survey region.

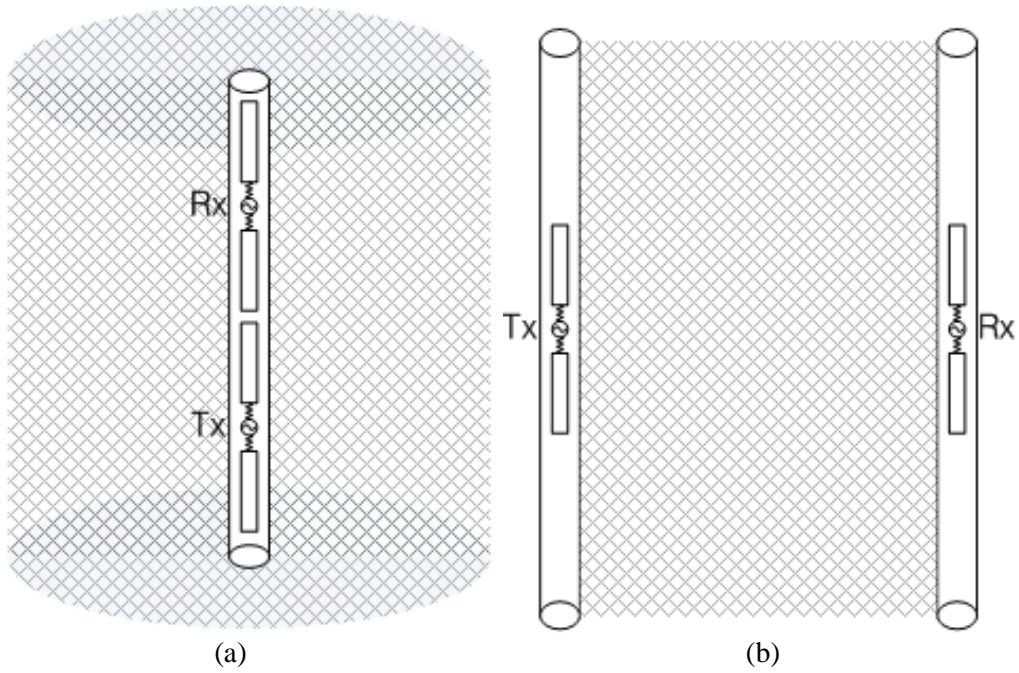


Fig.1.3 Performance with survey region of (a) single-hole radar (b) cross-hole radar.

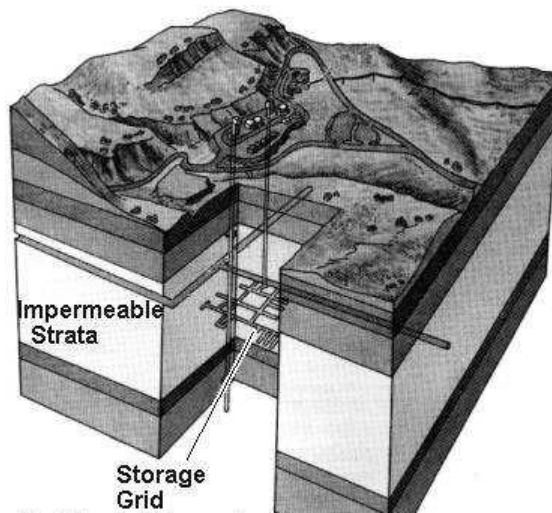


Fig.1.4 Nuclear waste disposal facility.

(http://www.geo.arizona.edu/palynology/geos210/lec_21.html)



Fig.1.5 SPR storage.

(<http://www.reuters.com/article/idUSN2328108920070124>)

1.2 Contents of dissertation

This research activity is concentrated on the development of GPR technique to monitoring fluid migration in porous material. There are two GPR techniques for different hydrogeological applications. One is the monitoring of preliminary experiment in the unconsolidated sand for the evaluation of hydraulic fracturing in the methane hydrate reservoir. Another is the monitoring of permeation experiment in the vadose zone for the estimation of migration model in the inhomogeneous media.

Chapter 1 is the introduction of GPR, and the thesis background and objective. Chapter 2 explains fluid migration in porous material which put on several conditions. Chapter 3 introduces measurement configurations applied to GPR experiments based on fluid migration in porous material. Specific signal processing methods are adopted each experiments in chapter 4. Chapter 5 suggests a migration modeling for verifying migration estimation. At final, the conclusion will be given in chapter 6.

Chapter 2

Principles of fluid migration in porous material

2.1 Fluid migration in unconsolidated sand

Preliminary experiment in the unconsolidated sand for the evaluation of hydraulic fracturing in the methane hydrate reservoir is conducted using a down-scaled specimen. The methane hydrate is a compound of methane and water under the specified pressure and temperature conditions as shown in Fig 2.1. It exists in the seabed sediment and under the arctic permafrost. Development mechanism of methane hydrate reservoir is different to conventional hydrocarbons. Methane is occurred in two ways. One is biogenic methane which is a byproduct of bacteria ingestion of organic material. Another is thermogenic methane which is a production of the combined action of pressure, temperature, and time on buried organic material. These methane migrate upwards due to its buoyancy relative to water, then change to methane hydrate at a place which satisfies the specified conditions. When methane hydrate fills the pores of sediment, it makes to reduce a permeability of sediment. It means that porous sediment turns into impermeable sediment, then works as a structural trap like salt dome.

Production method of methane hydrate is almost same to conventional hydrocarbons excavation. However additional techniques are required, because methane hydrate exists as a solid state. Hydraulic fracturing with depressurization, thermal stimulation or possibly solvent injection is designed to excavating methane hydrate efficiently. Evaluation of hydraulic fracturing in methane hydrate reservoir is difficult, because it is operated at several hundred meters below the seafloor. For this reason, down-scaled specimen is used a substitute for actual porous sediment.

During experiment, fracturing fluid selected single lubricant and mixed lubricants have different viscosities is used for hydraulic fracturing. When fracturing fluid is inserted steadily the same amount into a borehole, pressure of inner borehole is increased. Because fracturing fluid permeating into a specimen is difficult until an emission pressure of fracturing fluid reaches to breakdown which is a start-state to generate a fracture and to infiltrate fracturing fluid into a specimen [4]. After breakdown is occurred, fracture extends to a direction of the least horizontal stress, then fracturing fluid infiltrates into a specimen through a fracture corridor. There are three phases which are water, air, and fracturing fluid in a specimen. Fluid migration in a specimen indicates that variation of fluid movement and distribution by fluid dynamics and chemical reactions between these phases [5]. Small droplets of fracturing fluid invade into air occupied pores of specimen by pressure of fracturing fluid. At that time, an area with fracturing fluid occupied pores is called an infiltrated region. Air in an infiltrated region is pushed out of its own position, and then compressed to neighbor air occupied pores. In high pressure state, some compositions of air, especially oxygen, are easily dissolved in water. For that

reason, air migration from an infiltrated region to another region is less effect to a material distribution in a specimen. Water occupied pores are also invaded by fracturing fluid. Water droplets in an infiltrated region are migrated to pores in another region. At that time, water does not mix with fracturing fluid, and a volume of water is almost same even in high pressure state. Thus water migration from an infiltrated region to another region is quietly affected a material distribution in a specimen. Remain question is how to distribute fracturing fluid and water in a specimen during experiment. It will be mentioned in Chapter 5. Migration of fracturing fluid into a specimen makes to decrease an emission pressure of fracturing fluid. When an emission pressure of fracturing fluid is below the largest horizontal stress, a fracture generating is stopped and a fracture corridor is closed. It means that fracturing fluid cannot infiltrate into a specimen. After an experiment is finished, a specimen is cut horizontally or vertically to look at its cross-section, and then a fracture and an infiltrated region are determined as shown in Fig.2.2. Compare variation of an emission pressure of fracturing fluid with formation of a fracture and distribution of an infiltrated region, mechanism of hydraulic fracturing in the unconsolidated sand will be discovered. However, it is a fragmentary analysis, because there are no information about a fracture generation and an infiltrated region expansion during experiment.

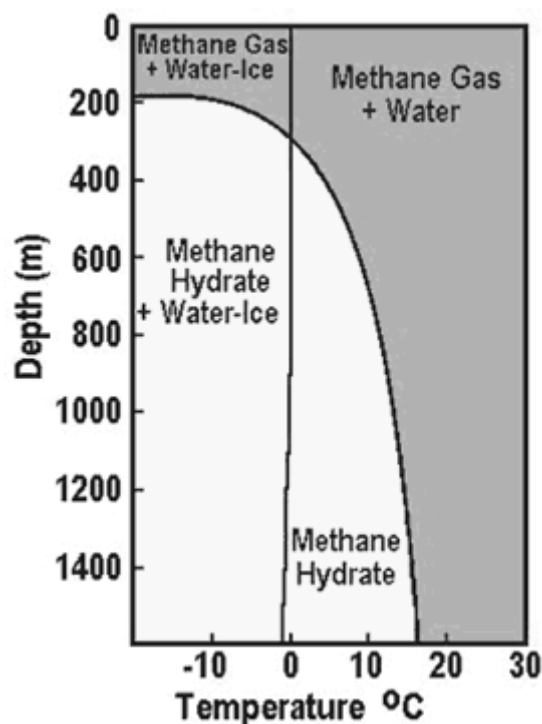


Fig.2.1 Methane hydrate phases.

(<http://www.netl.doe.gov/technologies/oil-gas/futuresupply/methanehydrates/about-hydrates/conditions.htm>)

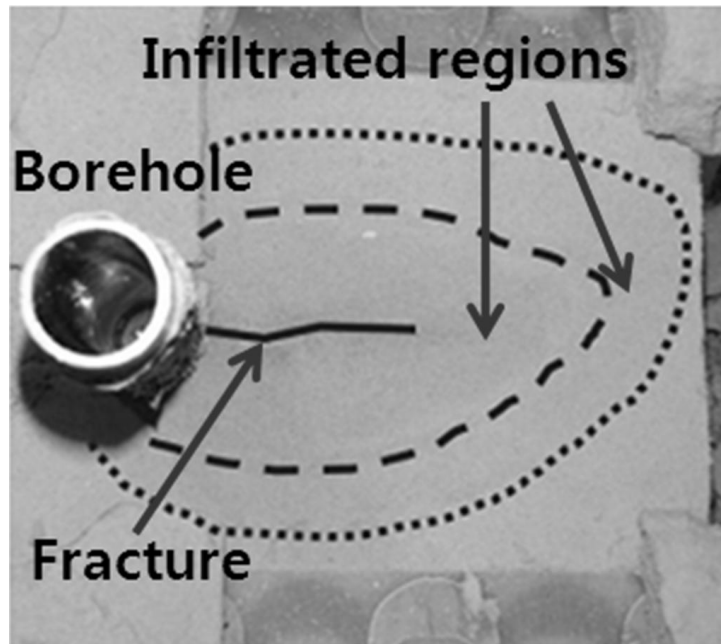


Fig.2.2 Cross-section of specimen.

2.2 Water migration in subsurface

Monitoring of the subsurface water migration for decision and surveillance a site of cellorage like nuclear waste disposal facility and SPR is conducted. Subsurface consists of substances which have different physical and chemical characteristics. There are several factors to affect these characteristics. One is a surface environment with different geographical positions. Climate like precipitation and temperature makes disintegration to the surface of the earth, and its phenomenon also affects the subsurface. Especially, short-term material migration is occurred through groundwater flow system. Another is a subsurface environment with different geological positions. Metamorphism by extremely high pressure and temperature varies subsurface materials physically and chemically. And long-term material migration like a diastrophism is happened by mantle convection. For several reasons, subsurface is generally an inhomogeneous media. It means that the subsurface water migration is an irregular flow and diffusion. There are several water migration models. These models estimate phenomena by microscopic-scale or macroscopic-scale approximations. Fundamental source of water dynamics is gravity. It means that water is forced to downside, except some special case like spring-water. When water is poured over the surface of the earth, it will start to infiltrate into the surface. This infiltration is related on the hydraulic conductivity of the material. Porosity and permeability of the material are affected to the evaluation of the hydraulic conductivity [6]. Relation between hydraulic conductivity and material characteristics is shown in Table 2.1. For example, solid granite itself has very poor porosity. Thus it is connected to low hydraulic conductivity. However if solid granite is highly fractured, its hydraulic conductivity is increased. Water contained or containable layer called the aquifer can be divided into two layers; confined and unconfined. Confined

aquifer underlies a confining layer which is a bed of low permeability called aquitard or an impermeable area called aquiclude. Amount of contained water in confined aquifer is conserved, but its quantity is very low. On the other hand, unconfined aquifer contains large quantity of water, but its amount of contained water is changed. Even position of unconfined aquifer is variable, because unconfined aquifer underlies water table. Thus a vestige of water migration is clearly investigated only at the unconfined aquifer and the unsaturated layer called vadose zone which exists above water table in nature. It will help to select a site of cellorage at unconfined aquifer or impermeable area especially. When a facility site is under construction, this artificial activity affects to groundwater flow system. At that reason, monitoring of the subsurface water migration is required.

Table 2.1 Saturated hydraulic conductivity (K) values found in nature.

K (cm/s)	$10 \sim 10^2$	$10^{-1} \sim 1$	10^{-2}	10^{-3}	10^{-4}	10^{-5}	10^{-6}	$10^{-8} \sim 10^{-7}$	$10^{-10} \sim 10^{-9}$
Relative permeability	Pervious		Semi-pervious				Impervious		
Unconsolidated sand & Gravel	Well sorted gravel	Well sorted sand or Sand & Gravel	Very fine sand, Silt, Loess, Loam						
Unconsolidated clay & Organic			Peat	Layered clay		Fat / Unweathered clay			
Consolidated rocks	Highly fractured rocks	Oil reservoir rocks			Fresh sandstone	Fresh limestone, Dolomite	Fresh granite		

Chapter 3

Configuration of GPR Measurements

3.1 Measurement of fluid migration

There are several geophysical measurement methods for exploration in the subsurface. Seismic methods, geodesy and gravity techniques, magnetic and electrical techniques, electromagnetic methods, and well logging are used for measuring parameters to define a material. Consider the experiment conditions mentioned in Chapter 2, transmission media is unconsolidated sand and blocked by metal plates. Unconsolidated sand is a porous material and its density is relatively lower than consolidated rocks. High density of material is proportional to high velocity of seismic wave. These factors affect to Q (Quality factor) which is an inverse value of an attenuation factor. Generally, low Q of transmission media corresponds to high porosity and low velocity in the seismic methods. Thus seismic wave in unconsolidated sand suffers from high intrinsic attenuation, and it leads to poor SNR (Signal to Noise Ratio). It is the same manner to acoustic and ultrasonic wave. Size of a specimen is relatively small to apply magnetic and electrical techniques, because a resolution of these techniques is poor to detect an area of fluid migrated region. Deployment of instruments which compress a specimen interrupts to conduct radioactive techniques. Consider SNR, resolution, and deployment of experiment, the most adequate geophysical measurement method in unconsolidated sand is an electromagnetic method. GPR is one of electromagnetic methods for geophysical measurement. Preparation, procedure, and methodology of GPR measurement are mentioned after sections.

3.1.1 Characteristics of the host material

The specimen consists of Tohoku silica, Kaolinite flour, and the distilled water. These materials are uniformly distributed into the mold and taken into a concrete hexahedron form by the exterior pressure. The completed specimen has almost 11 % volumetric moisture content and around 28 % porosity. These parameters cannot be directly measured by electromagnetic methods. Electromagnetic parameters of material are electric permittivity (ϵ), magnetic permeability (μ), and electrical conductivity (σ). Dominant electromagnetic parameter affected by volumetric moisture content and porosity of material is electric permittivity. When electromagnetic wave is propagating in medium, its velocity is depended on electric permittivity of medium as

$$v = \frac{c}{\sqrt{\epsilon_r}} \quad (3-1)$$

where c is the speed of light, ϵ_r is the relative permittivity of medium.

Acquiring electric permittivity of unconsolidated sand, antennas are inserted into a specimen. These antennas are connected to a calibrated VNA (Vector Network Analyzer) measurement system, and electromagnetic wave propagates in a specimen. Then VNA provides a travel time of propagating wave in a specimen in Fig. 3.1. The relative permittivity of medium is derived from a given equation as

$$\epsilon_r = \left(c \frac{(T_p - T_a)}{d} \right)^2 \cong 5.93 \quad (3-2)$$

where T_p is a travel time of propagating wave, T_a is a measured travel time in antennas, d is a distance between antennas.

Then using the Topp's equation with acquired the relative permittivity of medium, volumetric moisture content of medium is estimated [7] as

$$\epsilon_r = 3.03 + 9.3\theta_v + 146\theta_v^2 - 76.7\theta_v^3 \rightarrow \theta_v \cong 11.5 \% \quad (3-3)$$

where θ_v is the volumetric moisture content of medium.

Thus a suggested volumetric moisture content value is well estimated to a calculated volumetric moisture content value. It means that relation between the relative permittivity and volumetric moisture content in unconsolidated sand is followed to Topp's equation.

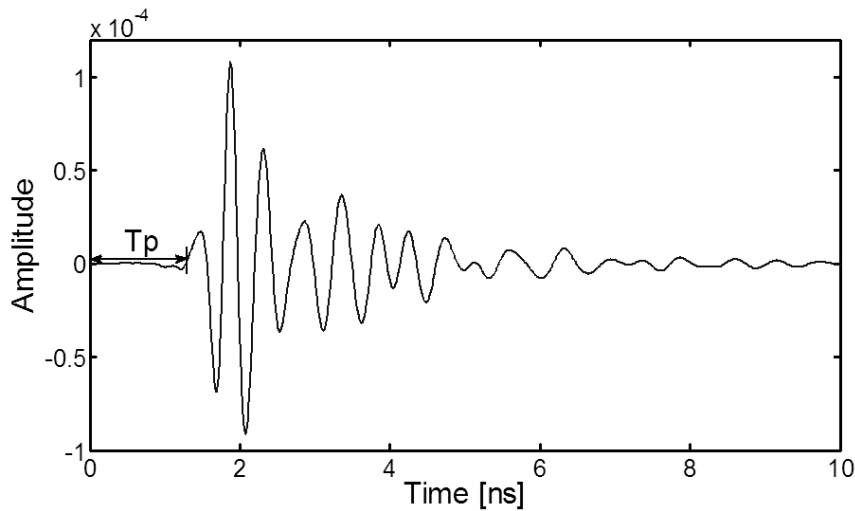


Fig.3.1 Waveform of received signal.

3.1.2 Characteristics of fracture fluid

Hydraulic fracturing was conducted by using Vitrea and Tellus (Synthetic lubricants, Shell). And red ink was used for visualizing the fracture. The required viscosity of a fracturing fluid is acquired by changing the ration of Vitrea and Tellus. The viscosity of Vitrea is larger than that of Tellus. Thus the

infiltration of Vitrea into the specimen is more difficult in comparison with Tellus. At that reason, Vitrea exists around near area of the developed fracture. On the other hand, Tellus spreads to farther area from the developed fracture. Although the particle size of red ink is relatively larger than the pore size of the specimen, its penetration from the fracture to the specimen is difficult. Hence red ink remains only in the fracture. The remained red ink in the fracture is useful for confirming the trace of the fracture. For measuring travel time of propagating wave in the each lubricant, a box is filled with each lubricant and attached antennas to face each other as shown in Fig. 3.2. The measured relative permittivity of Vitrea and Tellus are 2.13 and 2.19 using previous mentioned the same manner at 3.1.1. It implies that the electromagnetic characteristics of Vitrea and Tellus are almost same.

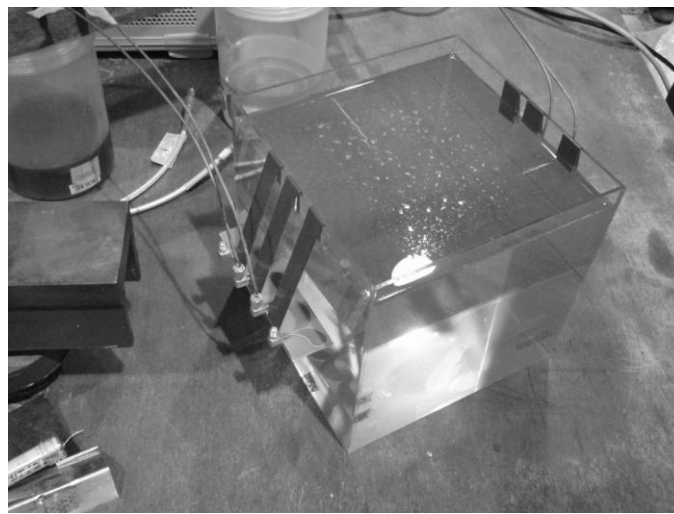


Fig.3.2 Fracturing fluid in a box to acquire its electric permittivity.

3.1.3 Method of hydraulic fracturing

In nature, tectonic stresses are put on the subsurface in all directions, and have relatively small difference between horizontal stresses except fault zone. Like that, specimen is also pressurized by compressors during experiment. Vertical stress (σ_v) and the largest horizontal stress (σ_H) are set to 2 MPa, and the least horizontal stress (σ_h) is set to 1 MPa as shown in Fig. 3.3. Then a borehole with slit is inserted into specimen vertically. At that time, slit is toward to the largest horizontal stress. Total volume of specimen is conserved during injection of fracturing fluid, because a specimen is pressurized by compressor and blocked by metal plates.

When fracturing fluid is inserted steadily the same amount into a borehole, pressure of inner borehole is increased. Geologist estimates that fracturing fluid permeating into a specimen is difficult until an emission pressure of fracturing fluid reaches to breakdown which is a start-state to generate a fracture and to infiltrate fracturing fluid into a specimen. After breakdown is occurred, fracture extends to a direction of the least horizontal stress, then fracturing fluid infiltrates into a specimen through a fracture corridor. After an experiment is finished, a specimen is cut horizontally or vertically to look at

its cross-section, and then a fracture and an infiltrated region are determined.

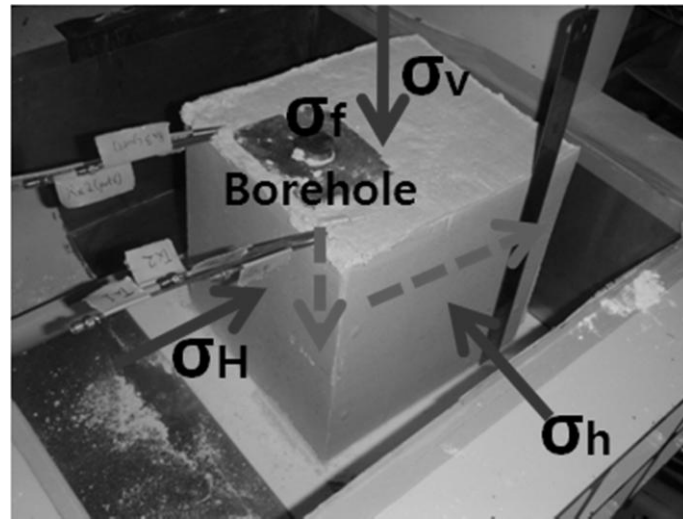


Fig.3.3 Test specimen for hydraulic fracturing.

3.1.4 Measurement system configuration

There are two typical GPR data acquisition methods. One is the time domain method using a pulse generator and an oscilloscope. The other is the frequency domain acquisition method using a VNA. The time domain acquisition method is able to fast signal acquisition, however its waveform may be unstable due to some jitters inherent in pulse generator. And sampling rate of oscilloscope affected upper boundary of frequency band is restricted to low value. Observation result of pulse generator signal is shown in Fig. 3.4. System delay is gradually decreased and does not stabilize. In contrast, the frequency domain acquisition is more stable because of its high SNR, but the data acquisition rate is relatively slow. In this experiment, the most important measurement value is the arrival time of receiving signal, because a propagation velocity corresponds to the formation of fracture and the infiltrated region on the propagating wave path.

In measurement system design, there are two requirement factors. One is the high spatial resolution. The fracture itself has a small aperture (≤ 1 mm) even in the open fracture condition when the pressure of the fracturing fluid (σ_f) is greater than the tectonic stress (σ_H). Thus an existence of fracture in the specimen using GPR measurement is not detected directly. However the expansion of the infiltrated region which fills with the fracturing fluid is detected by a variation of travel time at each propagation path. Based on the distribution of the infiltrated region, a formation of the fracture is estimated. Detection of this variation is required high spatial resolution. The other required factor is the acquisition rate. The pressure of a fracturing fluid varies drastically around breakdown pressure which is the peak pressure of a fracturing fluid, then the fracture may extend from the borehole in the direction of maximum horizontal tectonic stress (σ_H) and fracturing fluid infiltrated to outward around

the generated fracture. Since all of the above progress happens during a short time, its acquisition rate must be fast.

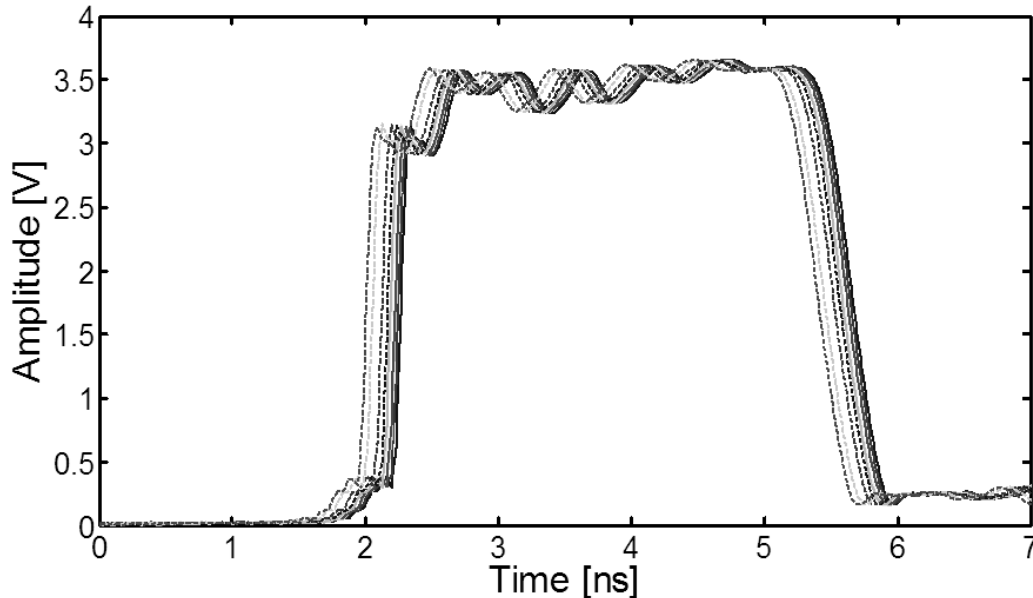


Fig.3.4 Observation result of pulse generator signal.

3.1.5 Vivaldi array antenna

Vivaldi antenna is a kind of twin-line UWB (Ultra Wide Band) antenna which has relatively high-gain and linearly polarization [8]. It has a wide frequency band, and its gain is stable with frequency varied. A single Vivaldi antenna element is designed and analyzed, and then arranged Vivaldi array antenna. It is used as transmitting and receiving antenna of 4x4 multi-static GPR for distribution measurement in the specimen. That antennas configuration is able to MIMO (Multiple Input Multiple Output) technique which helps to define characterizations of overlapped section of wave propagating paths, however 4x4 propagating wave paths are not enough to make a precise tomography of a fracture and the infiltrated region. Within several types of Vivaldi antenna, antipodal Vivaldi antenna is selected, because it is easy to fabricate metal patches and a feed. Vivaldi antenna element and Vivaldi array antenna are designed and produced. Those antennas are optimized by FDTD (Finite Difference Time Domain) simulation. Then the measurement and the simulation results are compared.

Vivaldi antenna element consists of two symmetrical metal patches which are confronted each other on the substrate [9], however feed of metal plates is different. Front and back side feed of metal plate has 1 mm and 7 mm width as shown in Fig. 3.5(a) and (b), because soldering connection between antenna and feeder must be strengthened. When antenna is inserted into the specimen, hand pumps give high pressure (2 ~ 3 MPa) to the specimen through metal plates. If antenna which has an optimized return loss in the operating frequency band (1 ~ 6 GHz) is considered, width of front and

back side feed is reduced. It leads that junction between antenna and feeder is easy to break. At that reason, return loss of Vivaldi antenna element is poor especially low frequency band in Fig. 3.6(b). Radiation pattern of H-plane is almost isotropic, but radiation pattern of E-plane has directivity to front and back side in Fig. 3.7(a) and (b).

Improving return loss at low frequency band and satisfying a requirement about antenna size, metal patches of Vivaldi array antenna are connected each other directly in Fig. 3.5(c) and (d) [10]. Length of metal patches is increased twice, however metal patches of port 1 and 4 are different each other. It makes an unbalance surface current. Neighbor ports are connected by metal patch. Its ends are connected inner conductor and ground of feeder. However mutual coupling is low, because ports of Vivaldi antenna array are connected with a switch driver which has enough isolation to do not interfere with each other in the operating frequency band. Increasing length of metal patches, electrical current of low frequency flows easier on the surface of metal patches. Thus it has a relatively good performance at low frequency in Fig. 3.6(a). Basically, radiation patterns of Vivaldi antenna element and Vivaldi array antenna are almost same, but E-plane of port 1 and 4 of Vivaldi array antenna is different because of its formation of metal patch in Fig. 3.7(a) and (b).

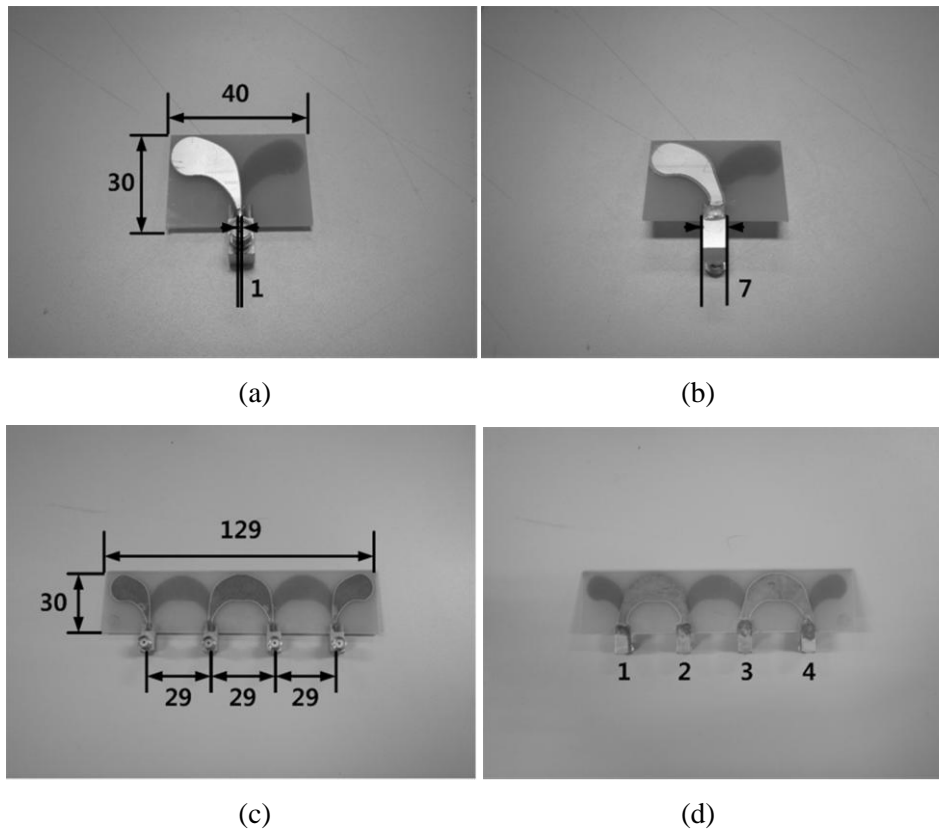
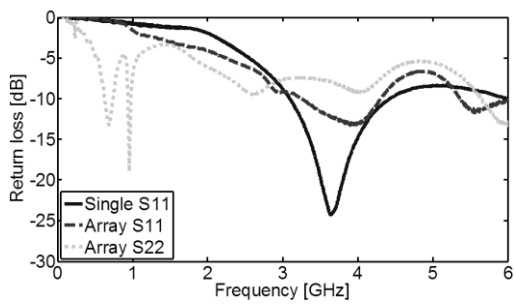
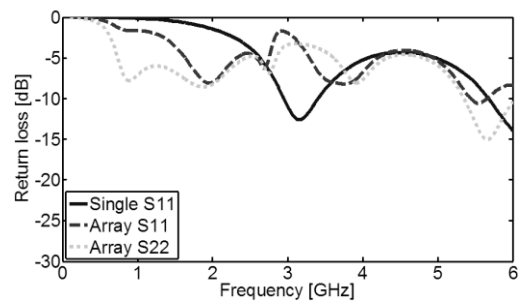


Fig.3.5 Vivaldi antenna element (a) Front side (b) Back side, Vivaldi array antenna (c) Front side (d) Back side, Unit = mm.



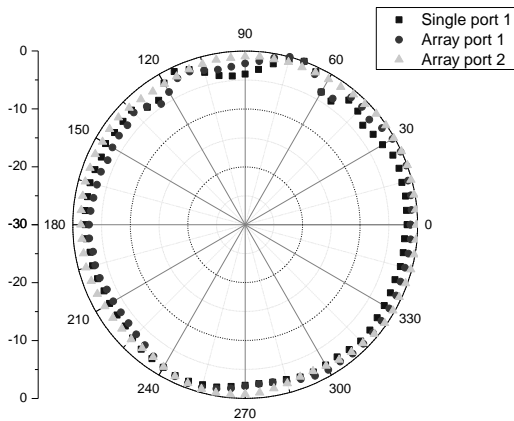
(a)



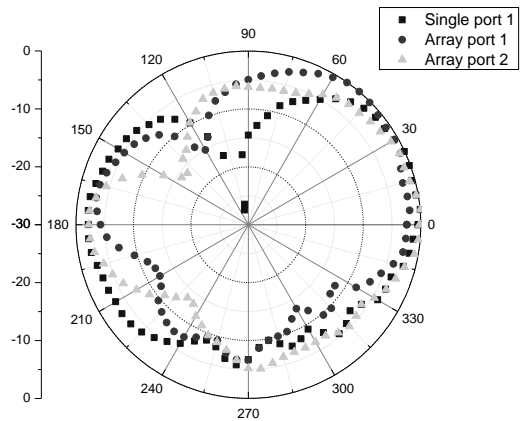
(b)

Fig.3.6 Return losses of Vivaldi antenna element and Vivaldi array antenna

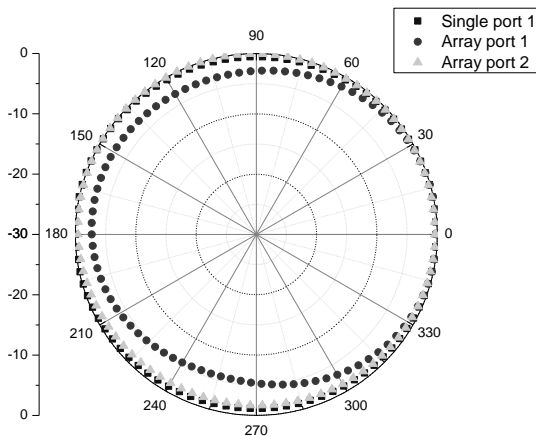
(a) Measurement (b) Simulation.



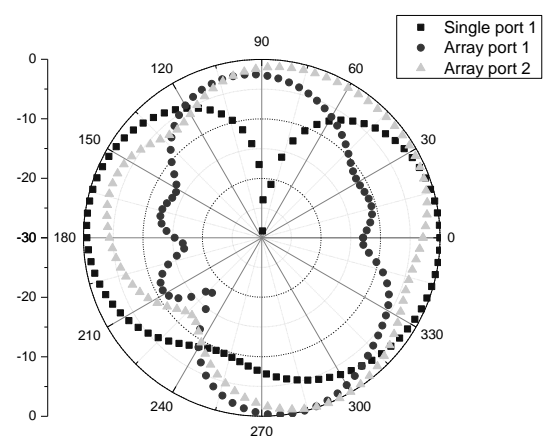
(a)



(b)



(c)



(d)

Fig.3.7 Radiation patterns of Vivaldi antenna element and Vivaldi array antenna at 3 GHz

(a) H-plane (Measurement) (b) E-plane (Measurement) (c) H-plane (Simulation) (d) E-plane (Simulation).

3.2 Measurement of water migration in Vadose zone

Acquiring the moisture content distribution, there are several methods like TDR (Time Domain Reflectometer) and Tensiometer used to measure volumetric moisture content. However these methods are restricted an application range within 1 m. Borehole radar is conducted deep-site surveillance, because the transmitting and the receiving antenna can be existed to deep-site through borehole. Compare with GPR (Ground Penetrating Radar) which has a measurement mechanism same as borehole radar, it has only few meter depth surveillance capability. It is a reason that the position of the transmitting and the receiving antenna is existed only on the ground surface.

Many papers were published to relate the monitoring of moisture content distribution [11] and water table level [12], however these papers proposed a measurement result elicited by ZOP (Zero-Offset Profiling) at specified depths. It means that acquired data provide only average value of volumetric moisture content with depth. Consider that water diffusion is an irreciprocal phenomenon in the subsurface, volumetric moisture content must be acquired to each specified positions.

3.2.1 Characteristics of Vadose zone

Measurement to monitoring of water migration in Vadose zone is conducted to Kanaya, Sizuoka, Japan. Experiment site exists in NIVTS (National Institute of Vegetables and Tea Science) laboratory as shown in Fig. 3.8(a). This area is a part of Makinohara-Daichi which consists of diluvial plateau. In a rough way, its soil has good drain characteristic. At that reason, this place is famous for the largest production site of green tea in Japan. The regolith covers with andosols and yellow soil, and sandy gravel bed layer exists under the regolith. Capillary fringe exists between sandy gravel bed layer and water table. Vadose zone consists of regolith, sandy gravel bed layer, and capillary fringe.

In the experiment, the regolith is removed, and then sandy gravel bed layer is exposed to the outside. Because the regolith has relatively poor drain characteristic than others, it makes difficult to measure equilibrium water content corresponded with inflow of water in sandy gravel bed layer.

3.2.2 Characteristics of migrated water

When water is infiltrated into the subsurface, electromagnetic characteristics of wave propagating path in the subsurface are changed. The subsurface water exists not only on a type of mixture, but also on a type of compound. Electric permittivity of the subsurface water is depended on a ratio of mixture. Volumetric moisture content is one of good indicator to explain a relation water migration with electric permittivity. However when water migrates in the subsurface, water is irregularly distributed. It means that each unit area of the subsurface has different volumetric moisture content. At that reason, the estimation of volumetric moisture content derived from a measured travel time of wave propagating path in the subsurface is indicated an averaged value. Electrical conductivity of absolute

pure water which consists of only H₂O molecules has 5.5 μS/m. However migrated water into the subsurface dissolves minerals like salinities, then its electrical conductivity is drastically increased to 0.05 ~ 0.5 S/m. Especially, migrated the subsurface water exposed excessive fertilizer has relatively high electrical conductivity. Attenuation of travel wave in the subsurface is affected by its electrical conductivity.



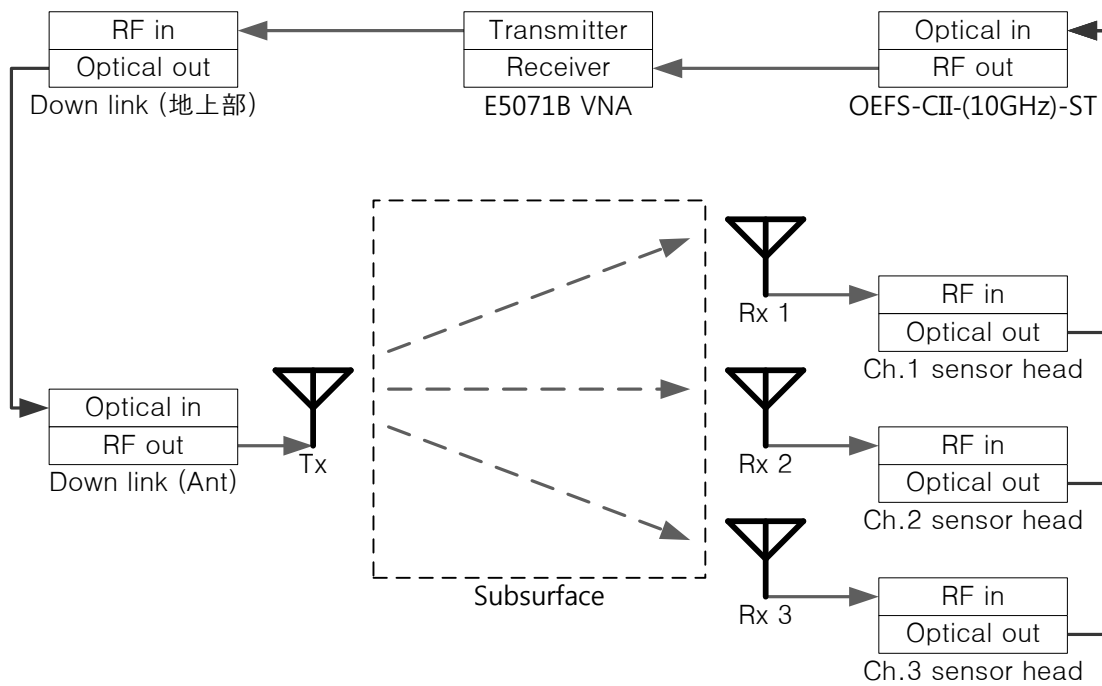
(a)



(b)



(c)



(d)

Fig.3.8 Borehole radar experiment

(a) A complete view (b) Measurement instruments (c) Antennas (d) System diagram.

3.2.3 Method of water injection

Water is selected a tap water which has relatively low salinity. Thus electrical conductivity of injected water is estimated to have a low value. Artificial increment of water salinity is achieved by an insertion of additional agent like sodium chloride into flowing water. However artificial control of water salinity is not conducted, because electrical conductivity of migrated water is not deterministically related to volumetric moisture content.

When water is poured into a pit, its flow rate per unit area is expressed as

$$C = \frac{Q}{A} = \frac{1.65 \text{ m}^3/h}{1.62 \text{ m}^2} = 1085 \text{ mm/h} \quad (3-4)$$

where Q is volumetric flow rate of injected water, A is an area of pit.

Water injection is continued 90 minutes, thus amount of total injected water is 2475 L. This experiment condition is not existence in nature. However it will help to acquire equilibrium water content which indicates a balanced flow state.

3.2.4 Measurement system configuration

Measurement system diagram is show in Fig. 4.8(b). An operating frequency of measurement system is selected by composition of the subsurface materials, because an attenuation of transmission media is drastically increased in proportion to frequency increment. Although operating frequency band must be as low as possible, measurement system must have wide frequency bandwidth. It makes to improve a time resolution which is able to discriminate multiple-path waves. SNR is important parameter in this measurement system, because transmission media in the subsurface affects amplitude and delay of travel wave.

Frequency bandwidth is only variable parameter in the measurement operation, its value is changed by IF (Intermediate Frequency) bandwidth of VNA. For improving SNR, IF bandwidth must be reduced. Improvement of SNR and processing velocity are a trade-off relation. In this experiment, acquisition time is less important, because water migration velocity is relatively slow within detectable variation range. Thus measurement system configuration is pursued high dynamic range to acquire high SNR.

3.2.5 Dipole array antenna

As mentioned earlier at 3.2, 1-D (Dimensional) measurement like ZOP is not sufficient to acquire horizontal moisture content distribution. It means that an inclination angle of migrated the subsurface water is not derived. At that reason, receiving antenna is adopted array deployment to measure an inclination tendency of the moisture content distribution. Typical borehole radar adopts dipole antenna, because an inserted antenna should be considered the borehole structure restrictions. Representative

structural parameter affected antenna characteristics are length of antenna. Its value is not limited by borehole structure and decides resonance frequency of dipole antenna as

$$f_c \approx \frac{c}{2l_{eff} \sqrt{\epsilon_r}} \quad (3-5)$$

where l_{eff} is an effective length of dipole antenna, ϵ_r is a relative permittivity of surrounding media.

This experiment adopts a cylindrical dipole antenna for transmitting antenna, and rod-type dipole antennas for receiving array antenna as shown in Fig. 3.9 (a) and (b). Basically, these antennas have resonance frequencies corresponded to lengths of antenna. However acceptable bandwidth of antennas defined its return loss (Usually ≤ -10 dB) is different, because its value is dominantly depended on the l/d ratio. The evaluation of acceptable bandwidth is expressed as

$$\frac{f_{upper} - f_{lower}}{f_c} \times 100 \% \quad (3-6)$$

where f_{upper} is a upper boundary frequency of bandwidth (≤ -10 dB), f_{lower} is a lower boundary frequency of bandwidth (≤ -10 dB), f_c is a center frequency.

Generally, diameter of antenna and input impedance of antenna are inverse proportion relation at fixed length of antenna. And feeder of cylindrical dipole antenna has tapered structure. Thus cylindrical dipole antenna has larger acceptable bandwidth than rod-type dipole antenna in Fig. 3.10.

These antennas are inserted into sondes which protect antenna from ground water and outthrust of borehole. At that time, deployment of antenna array elements is 1 m spacing between antenna feeders vertically. Consider radiation pattern of dipole antenna in Fig. 3.11, mutual coupling between antenna array elements does not strongly affect each other.

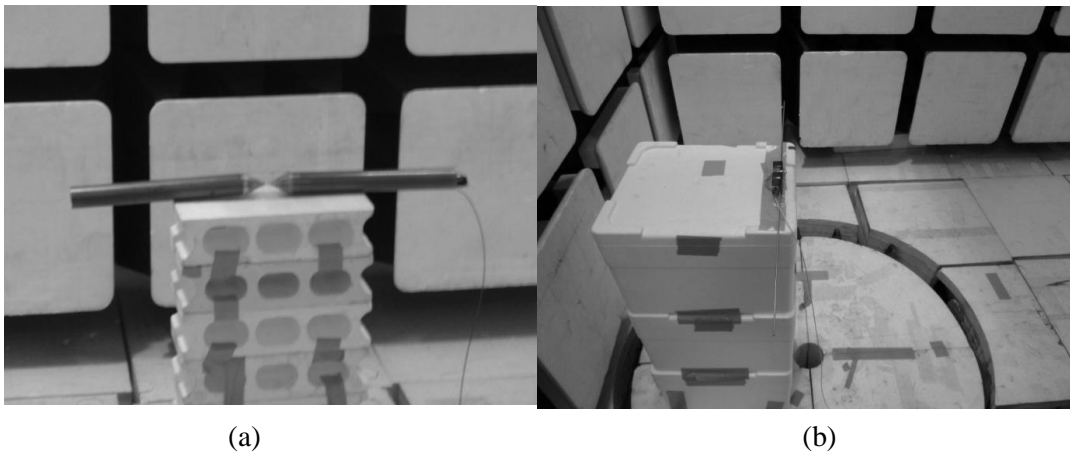


Fig.3.9 Appearance of dipole antennas (a) Cylindrical dipole antenna (b) Rod-type dipole antenna.

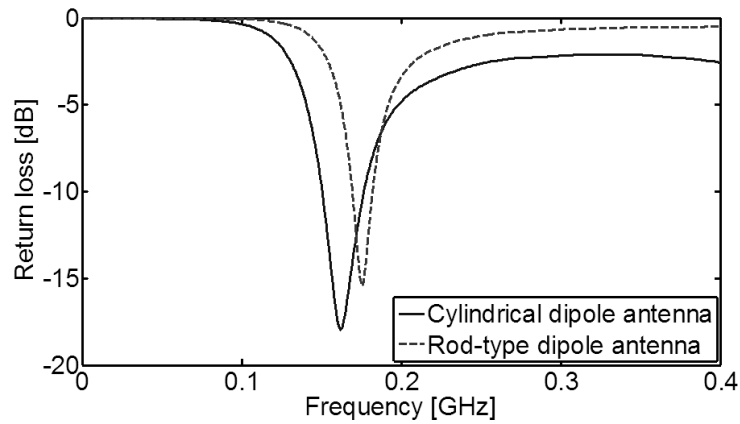


Fig.3.10 Return loss of dipole antennas.

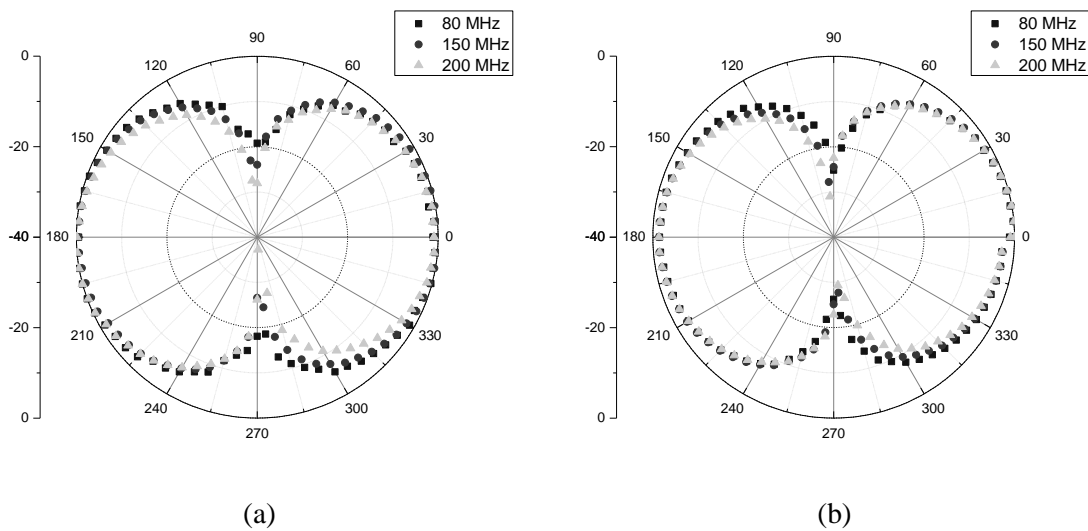


Fig.3.11 Radiation pattern of a dipole antenna (E-plane)
 (a) Cylindrical dipole antenna (b) Rod-type dipole antenna.

3.2.6 Optical link system

In this experiment, antennas are connected measurement instruments by optical link system as shown in Fig. 3.12 (a) and (b). Optical link system is divided two conversion modules converted electrical signals to optical signals and vice versa. Compare with electrical transmission, optical transmission has better performances which are attenuation and dispersion of transmitted signals. And optical fiber cable consists of dielectric materials. At that reasons, it is difficult to radiate any waves from optical fiber cable to the subsurface.

Before conduct field experiment, performance of an optical down link and an optical sensor must be tested. Measuring above mentioned things, the operating frequency is selected to 30 kHz ~ 1 GHz. An optical down link has almost 70 dB amplified gain and flatness within 700 MHz in Fig. 3.13(a). An optical sensor has almost 5 dB amplified gain and flatness given frequency band in Fig. 3.13(b). Thus

our measurement system provides almost 75 dB amplified gain and flatness within 700 MHz. Signal transmission of optical link system is nonreciprocal, because it is not equipped optical duplexers. Thus calibration of measurement system is incomplete, because VNA cannot conduct full 2 ports calibration. In the addition, optical sensors have no 50 Ω connectors. At that reason, only RF parts of measurement system is calibrated. Although optical link system is not calibrated directly, there is a method to calibrate optical link system indirectly.



Fig.3.12 Optical link system (a) Down link (Antenna) (b) An optical probe.

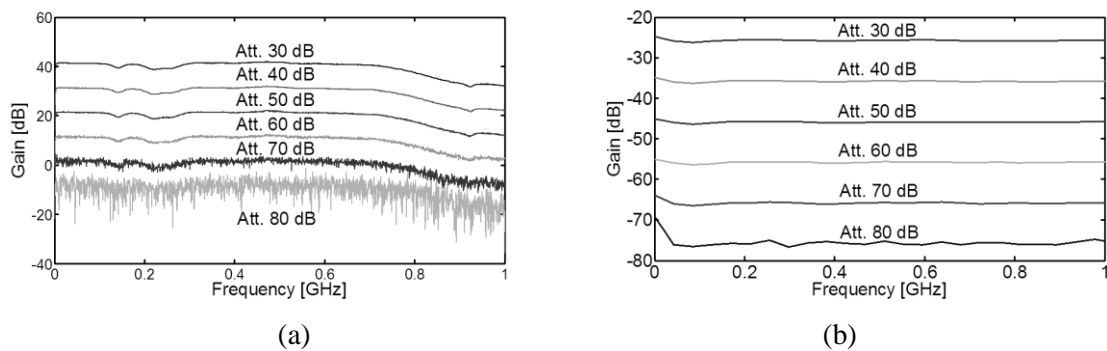


Fig.3.13 Power spectrum of optical link system with attenuation
(a) Optical down link (b) Optical probe.

3.2.7 Evaluation of measurement system

Using optical link system, transmission measurement of dipole antennas is conducted in an anechoic chamber. At that time, a junction between optical link system and dipole antenna should be inserted attenuator, because reflection is occurred at a junction. Strong reflection makes a ringing which is unwanted oscillated signals. Attenuator connected at junction reduces reflected signal power.

Measurement result is well matched to simulation result in Fig. 3.14. Even distortion and attenuation of signal is reduced using optical link system, significant frequency band is restricted within 80 MHz

~ 500 MHz. However previous frequency band covers frequency range for borehole radar, there is no problem to adopt dipole antennas with optical link system to borehole radar.

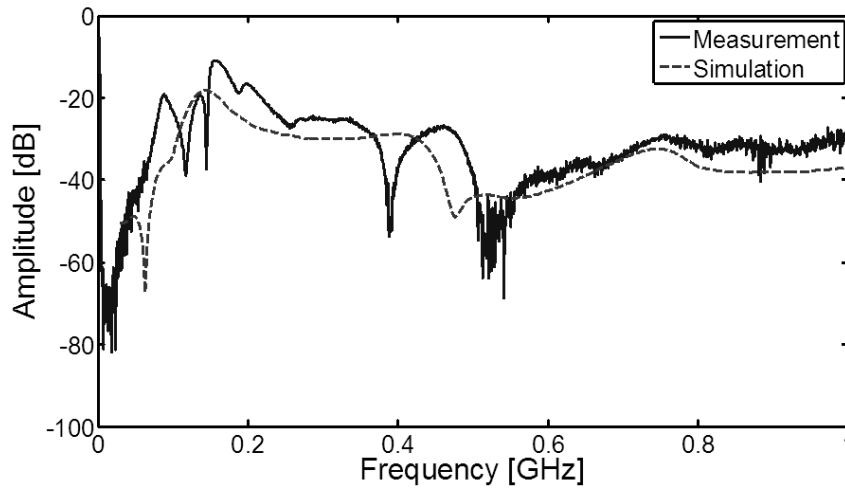


Fig.3.14 Transmission between dipole antennas.

Chapter 4

Experiments

4.1 Monitoring of fluid migration in a sand specimen

Comparing the actual formations of the fracture and the infiltrated region with the pressure of fracturing fluid, the extension of the fracture is verified indirectly. At the same time, a diffusion of the fracturing fluid and a condensation of the moisture are measured. When the fracturing fluid infiltrated into the specimen, the fracturing fluid invaded not only to the empty pore but also to the pore which is occupied by the moisture. Hence the moisture is forced out and moves to the empty pore near the outer boundary of the region. It may be possible to understand the relation between the pressure of the fracturing fluid and the formation of the fracture in real time.

One of important factors on improving the production efficiency of these methods may be how to survey the formation of the fracture and the infiltrated region [13]. However, a preliminary hydraulic fracturing experiment in the laboratory using down-scaled specimen is not easy to determine the real-time development of fracture and the infiltration of fracturing fluid due to the variation of fracturing fluid pressure in borehole. It is possible to observe the formation of fracture and the infiltrated region only after cutting the section of the specimen as shown in Fig. 4.1.

As a detour, the GPR measurement system provides the variation of the travel time of received electromagnetic signals. Hence these signals make it possible to observe the real-time development of a fracture. And this method may be applied to monitoring the formation of a fracture and the infiltrated region for methane hydrates. Finally this method renders it possible to survey the fracture development for geothermal power generation and the exploitation of ground water.

For the experiment about monitoring the formation of fracture and the infiltrated region in the laboratory, a down-scaled specimen is used and an appropriate measurement technique is prepared [14]. Compared to actual subsurface reservoir, the specimen is small. GPR is a good technique for this experiment because of its relatively high frequency and wide frequency bandwidth. It means that GPR has a relatively superior time resolution than other geophysical applications. To obtain the reliable variation of the arrival time which corresponds to the formation of fracture and the infiltrated region on the propagating wave path. In this reason, the frequency domain acquisition methods are applied to this experiment. Specifications of measurement are listed in Table 4.1.

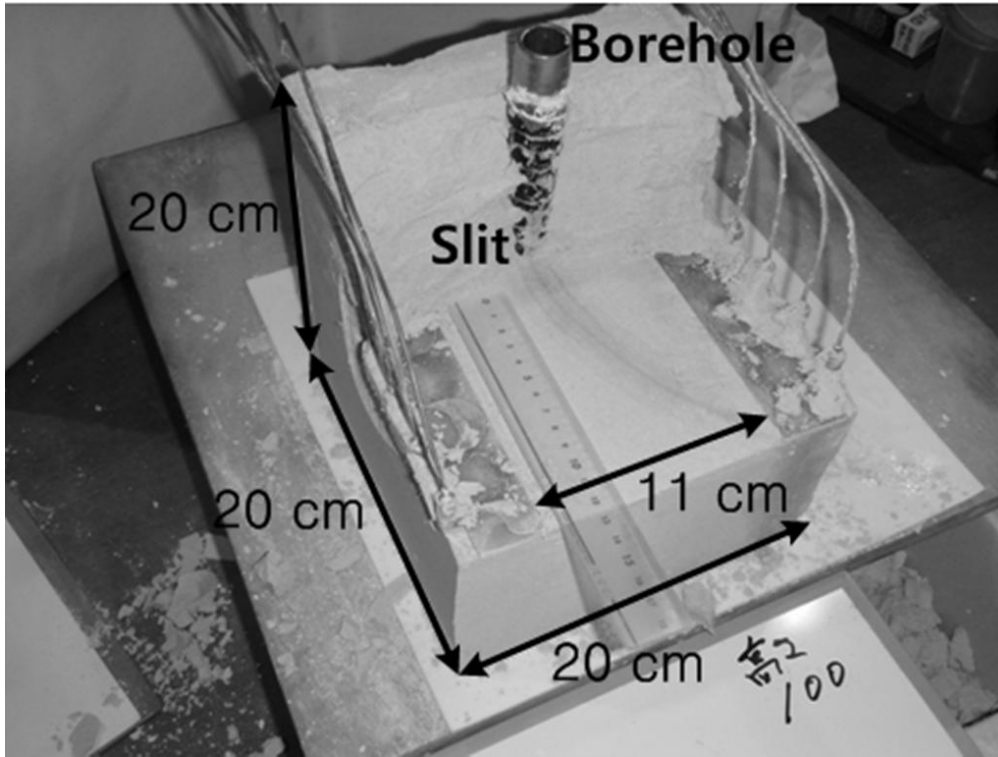


Fig.4.1 Inner structure of specimen.

Table 4.1 Specifications of measurement.

Specification	Value	Remark
Frequency	300 kHz ~ 6 GHz	Operation
Number of points	201	-
IF bandwidth	100 Hz	-
Acquisition time	0.72 sec	A propagating wave path
Injecting rate	30 ml/min	Fracturing fluid
Viscosity	1700 mPa·s, 300 mPa·s	Single (Vitrea), Mixed (Vitrea with Tellus)
Porosity	28 %	Specimen
Volumetric moisture content	11 %	Specimen

4.1.1 Experiment results

Hydraulic fracturing experiments using down-scaled specimen are conducted many times. Early experiments are conducted to evaluate measurement systems and antenna deployments. For example, several experiments are tried to find a proper data acquisition time satisfied both data quality and tracking of media variation at the same time. On the other hand, time domain measurement using pulse generator and oscilloscope is attempted. Based on the results of these preliminary experiments, controlled measurement circumstance to acquire effective and well-directed data is prepared.

When Vivaldi array antennas are placed in the specimen, ports of each antenna are labeled. Based on

the homogeneity of transmission media and the reciprocity of measurement system, signals acquired by simplex method are enough to represent whole acquirable signals. At that result, 16 propagating wave paths are selected, and then classified 4 types by its distance. At the same reason, acquired travel times corresponded each propagating wave path are compensated with initial travel time represented initial state, because that will be skip over system calibration which occupies a considerable portion of acquisition time.

The configuration of measurement system is set as show in Fig. 4.2. The synchronization of acquisition data which pressure of fracturing fluid and travel times is important to examine relation between pressure of fracturing fluid and the fluid migration with the fracture generation.

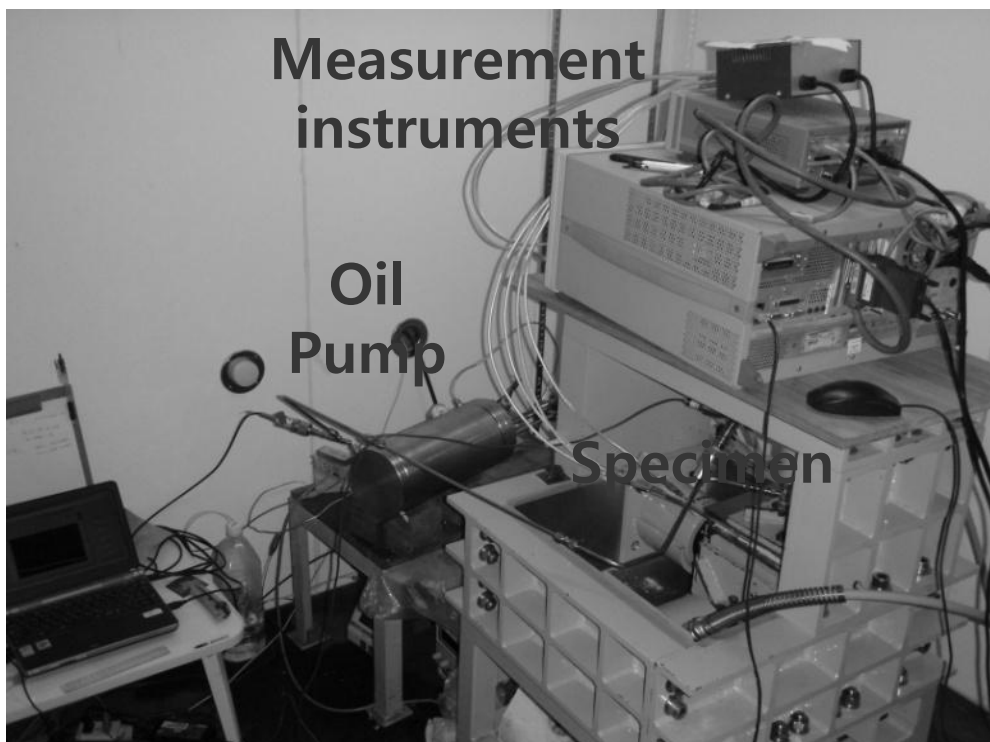


Fig.4.2 Configuration of measurement system.

Experiment with Mixed fracturing fluid (Vitrea and Tellus)

After the fracturing fluid is pressurized in Fig. 4.3, a fracture and infiltrated regions at the experiment finished state are determined by cutting a specimen as shown in Fig. 4.4. At that time, 4 classified propagating wave paths are arranged by schematic diagrams as shown in Fig 4.5(a)-(d). When the pressure of fracturing fluid is increased until reached to breakdown, there is no meaningful variation of the travel time in Fig. 4.6(a)-(d). After the breakdown, the pressure of the fracturing fluid is decreased abruptly and then stabilized. The stabilized pumping pressure is called the fracture propagation pressure. At the same time, the fracture grows in the forward direction, and the fracturing fluid is also infiltrated into the specimen through the developed fracture path [15]. At that

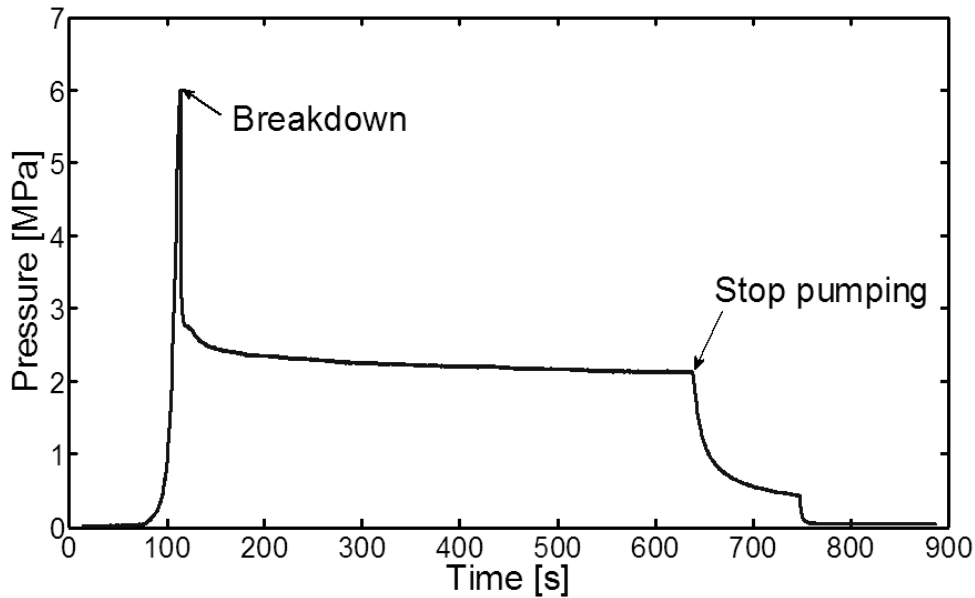


Fig.4.3 Pressure of mixed fracturing fluid.

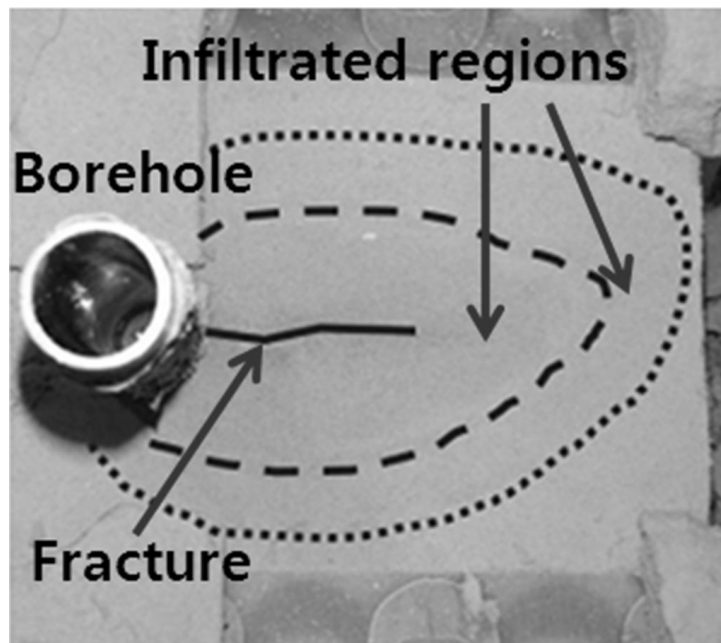


Fig.4.4 Cross-section of specimen.

time, the travel time of each propagating wave path is changed drastically. One of interesting features is that the variation of the travel time of each propagating wave path may be categorized into two groups. One group shows the velocity of propagating wave to be accelerated like T51 and T62 in Fig. 4.6(a). In contrast, the other group suffers from reducing the velocity of the propagating wave like T73 and T84 in Fig. 4.6(a).

The arrival times corresponding to each propagating wave path are well matched to the sequence of the propagating wave path close to the borehole, because the infiltrated region is expanded across area

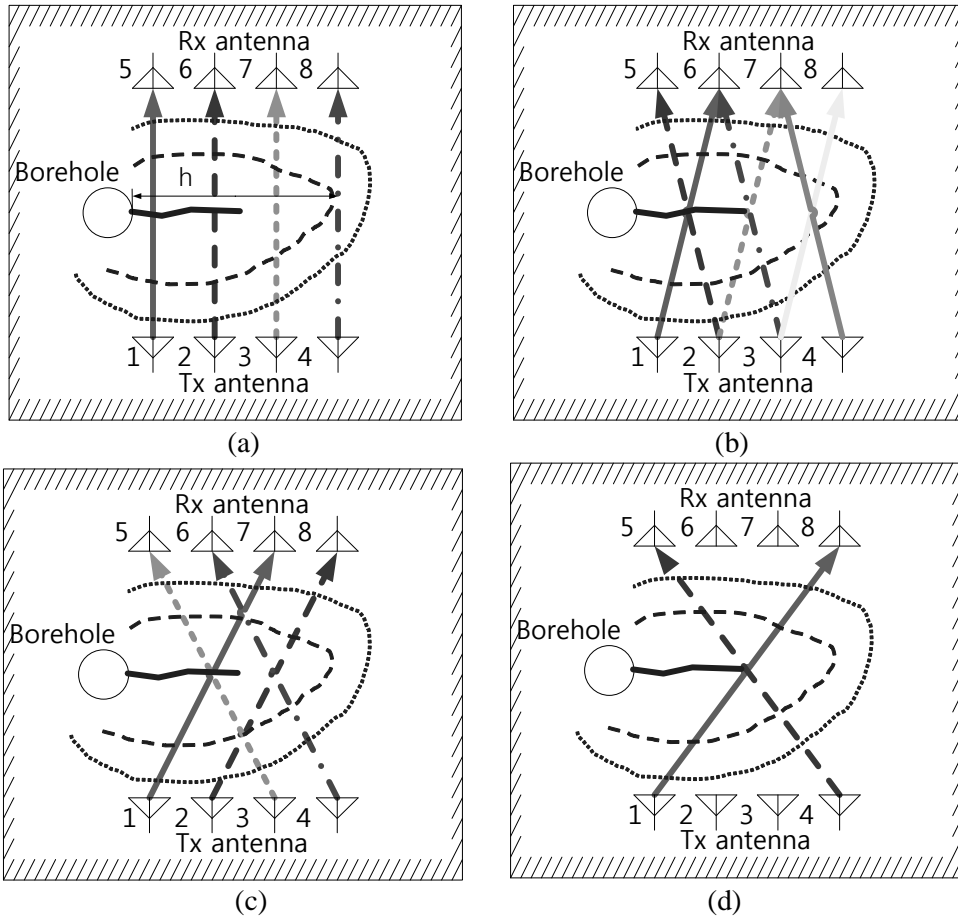
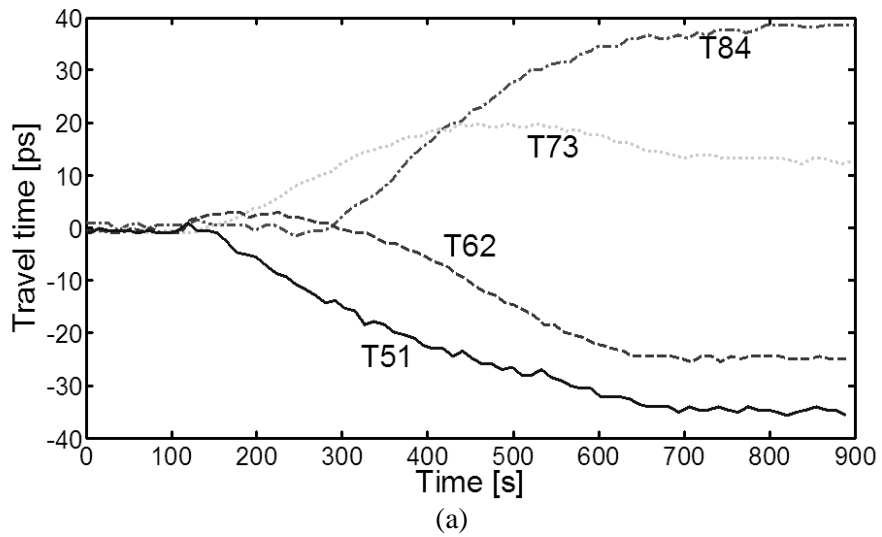


Fig.4.5 Schematic diagrams of propagating wave paths which have a distance
 (a) 11 cm (b) 11.40 cm (c) 12.53 cm (d) 14.21 cm.



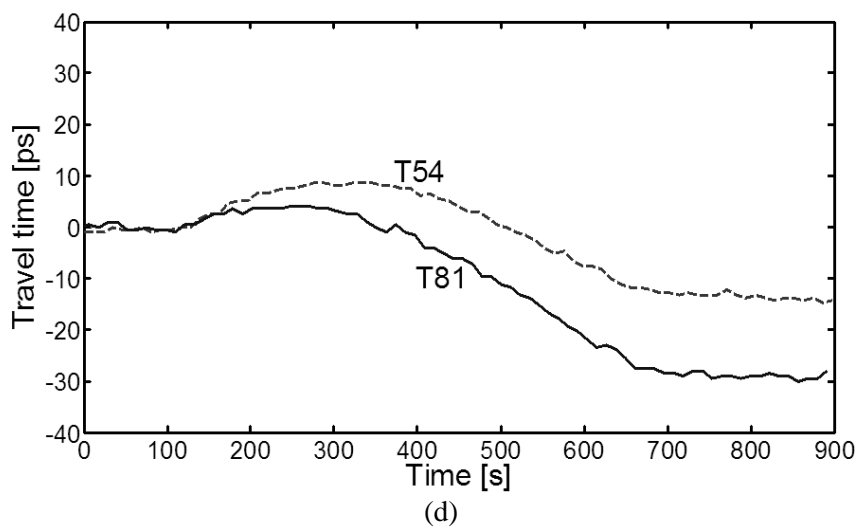
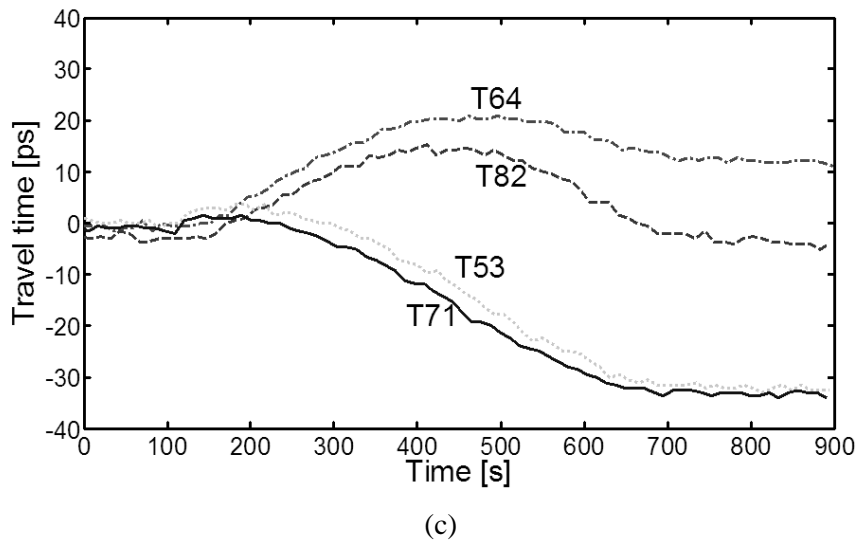
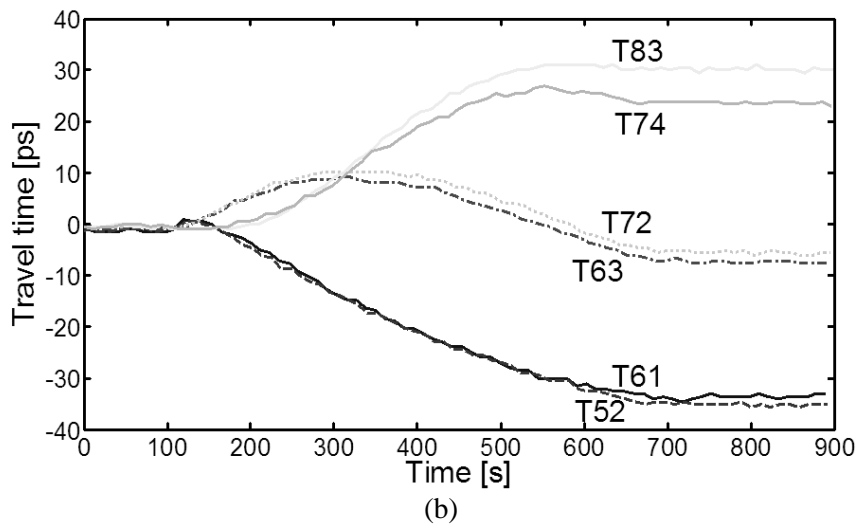


Fig.4.6 Travel times to propagating wave paths which have a distance (a) 11 cm (b) 11.40 cm (c) 12.53 cm (d) 14.21 cm.

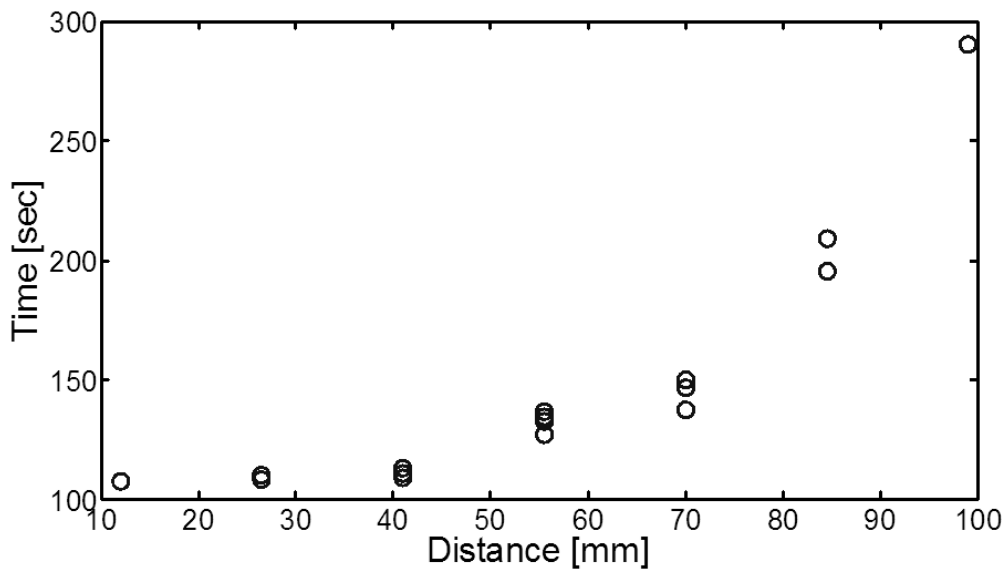


Fig.4.7 Arrival time of the infiltrated region.

between antennas and propagating wave paths are represented as simple closed curves. Developing velocity of the infiltrated region is inversely proportional to distance h from the borehole to contact intersection of the infiltrated region and the propagating wave path in Fig. 4.7. Although flow rate of the fracturing fluid is maintained a constant value, boundary of infiltrated region is increased. Thus relative compressed power to outer boundary of infiltrated region is decreased. Compare Fig. 4.3 with Fig. 4.7, it is also explained by the relation between pressure of fracture fluid and arrival time of fracturing fluid.

When the pumping is stopped, the pressure of the fracturing fluid decreases and soon becomes lower than the tectonic stress. At that time, there are no developing of the fracture and infiltrating into the fracturing fluid, because the fracture does not maintain the open state and turns into the close state. Thus the variation of the travel time does not exist in Fig. 4.6(a)-(d). The relative permittivity of the fracturing fluid is lower than that of the specimen. Considering the whole travel times of the propagating wave paths, the tendency of the travel times depends on the closeness from the borehole. The propagating wave path close to the borehole provides a strong downward tendency. It implies that the propagating wave velocity is increased. On the other hand, the propagating wave path stayed away from the silt, its tendency shows in the upward direction. Considering only the existence of the fracturing fluid, this upward tendency is physically impossible. This abnormal phenomenon can be explained if the relative permittivity of the infiltrated region increases. Additional explanation is mentioned to Chapter 5.

Experiment with Single fracturing fluid (Vitrea only)

To observe more apparent the development of fracture, an experiment with single fracturing fluid (Vitrea) is conducted. Compare the pressure of fracturing fluid with previous data in Fig. 4.3, even experiment is conducted to the same conditions, high viscosity characteristic of the fracturing fluid makes to increase the breakdown pressure 6 MPa to 8 MPa and reduce the fracturing time 520 seconds to 210 seconds in Fig. 4.8. It means that the generation of fracture using high viscosity fracturing fluid is required high initial pressure, but the expansion velocity of fracture is increased. Because of its own viscosity characteristic, infiltrated region is restricted within near fracture as shown in Fig. 4.9. At that time, 4 classified propagating wave paths are arranged by schematic diagrams as shown in Fig. 4.10(a)-(d). When the pressure of fracturing fluid is increased until reached to breakdown, there is no meaningful variation of the travel time in Fig. 4.11(a)-(d). Fundamentally, the direction of fracture generation is decided a low pressure area around the end of fracture. Given the exterior tectonic stress condition is enforced to whole specimen surface uniformly, fracture is generated straightforward as shown in Fig. 4.4. On the other hand, the direction of fracture generation is varied as shown in Fig. 4.9. It affects the pressure of fracturing fluid to increase during the fracturing. This phenomenon can be seen after 280 seconds from experiment start as shown in Fig. 4.8. When the direction of fracture generation is tilted, front surface of fracture formed to breakthrough specimen is enlarged. It makes to increase a pressure for fracturing. Thus the pumping is stopped, even the pressure of fracturing fluid is not approached to σ_H (=2 MPa). At that time, the variation of the travel time of each propagating wave path is also categorized into two groups. One group shows the velocity of propagating wave to be accelerated like T51 in Fig. 4.11(a). In contrast, the other group suffers from reducing the velocity of the propagating wave like T62, T73, and T84 in Fig. 4.11(a). The

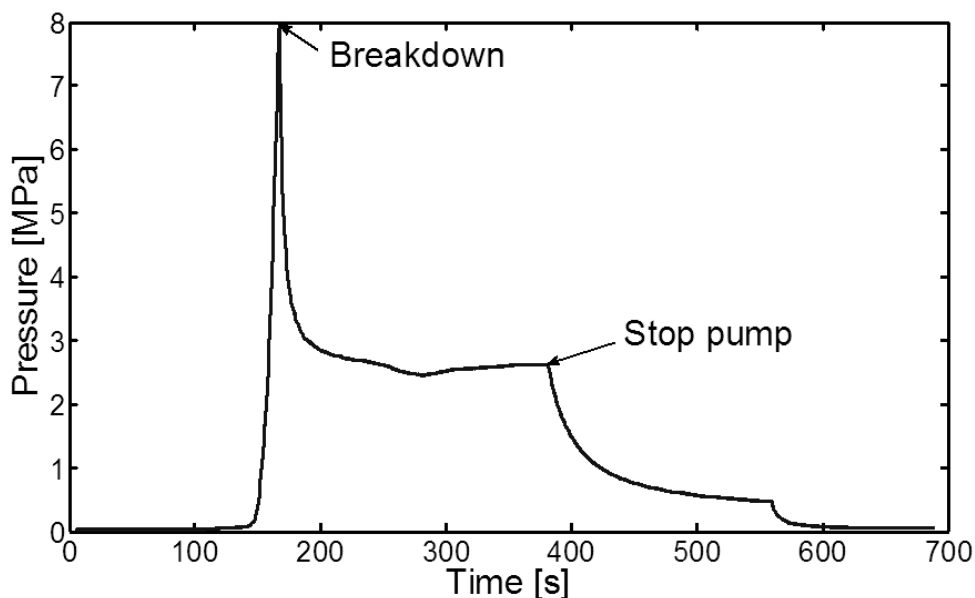


Fig.4.8 Pressure of mixed fracturing fluid.

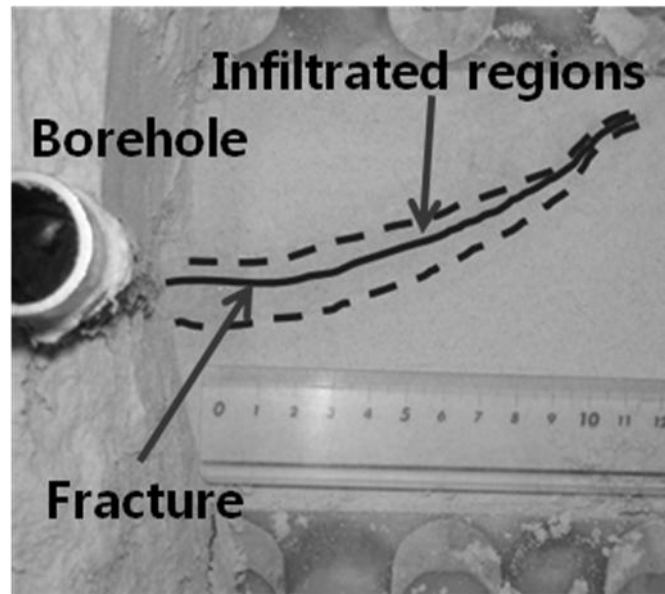


Fig.4.9 Cross-section of specimen.

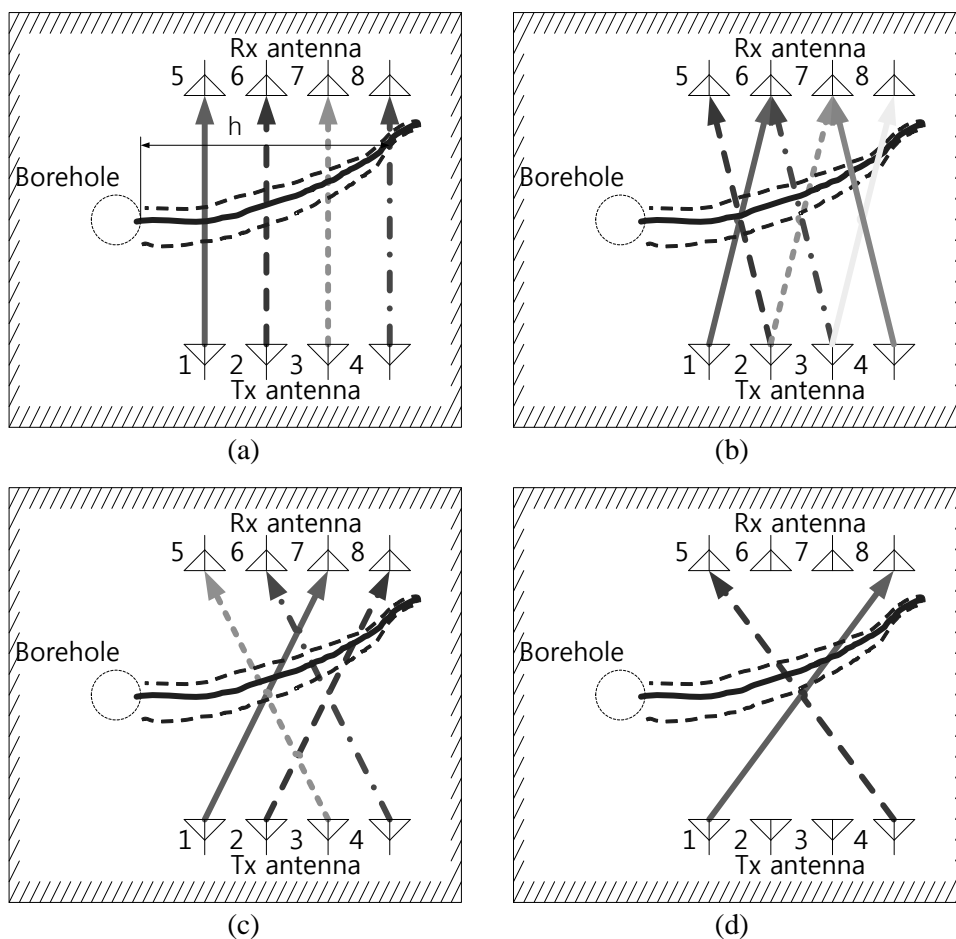
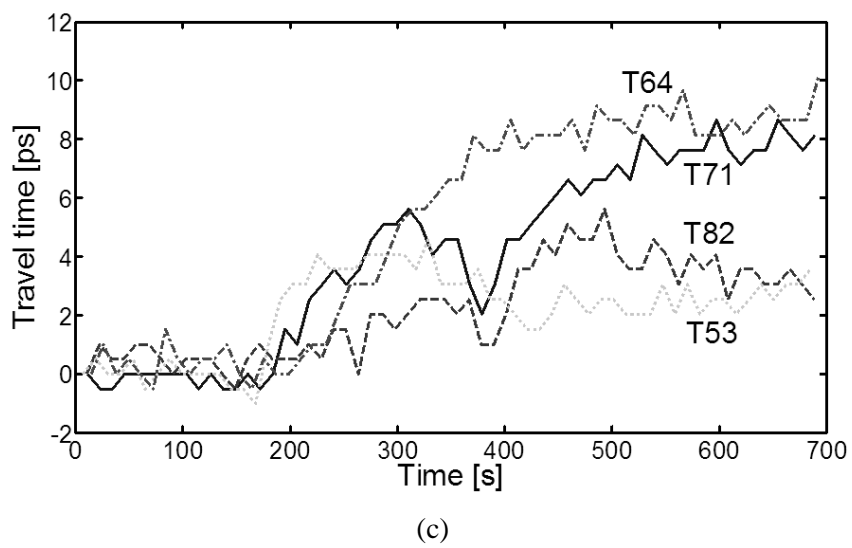
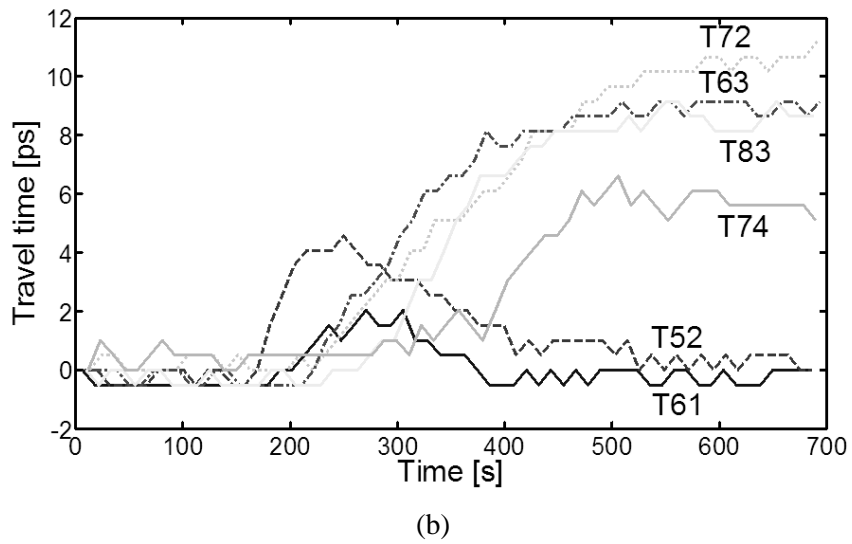
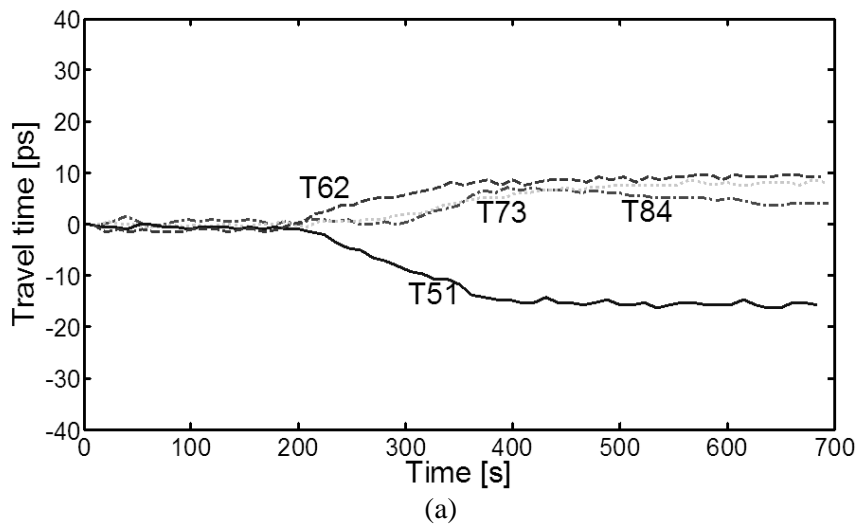


Fig.4.10 Schematic diagrams of propagating wave paths which have a distance
 (a) 11 cm (b) 11.40 cm (c) 12.53 cm (d) 14.21 cm.



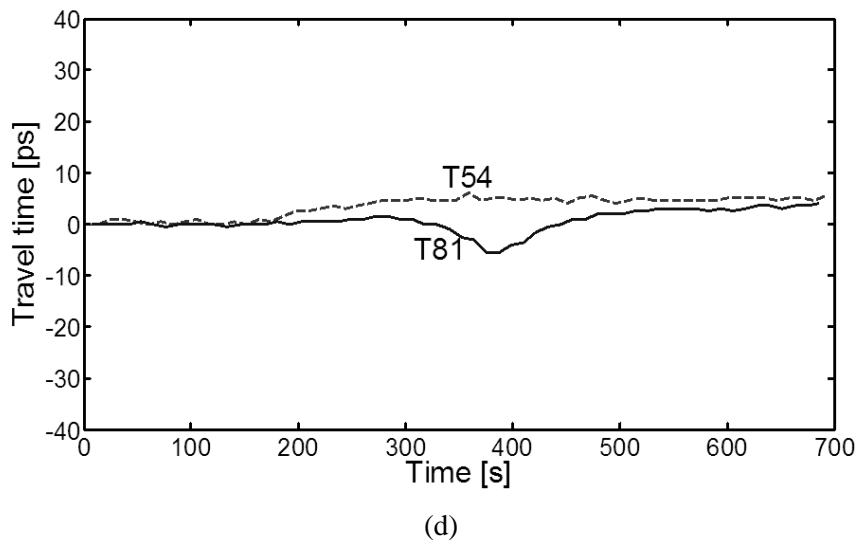


Fig.4.11 Travel times to propagating wave paths which have a distance
 (a) 11 cm (b) 11.40 cm (c) 12.53 cm (d) 14.21 cm.

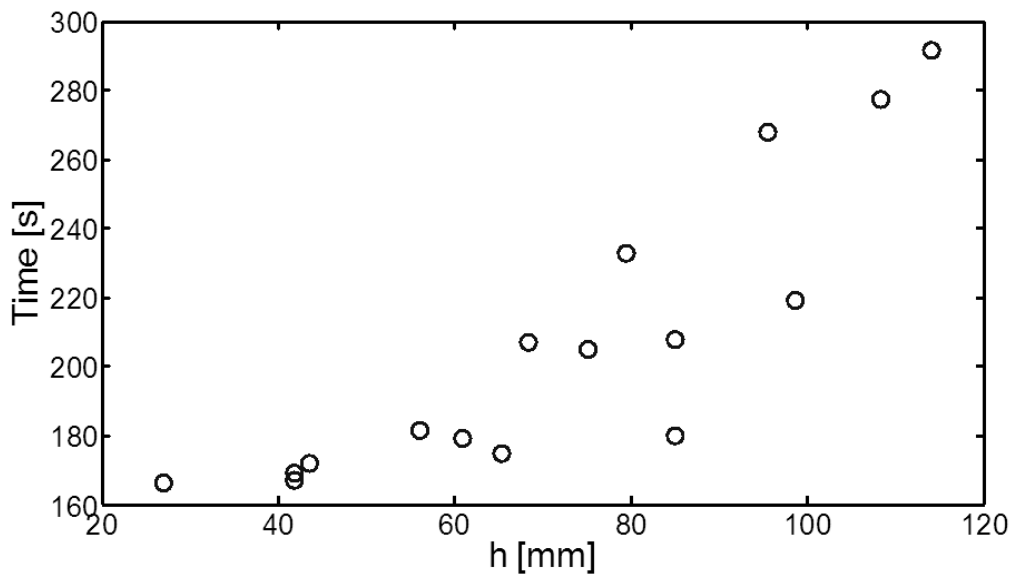


Fig.4.12 Arrival time of the infiltrated region.

arrival times corresponding to each propagating wave path are well matched to the sequence of the propagating wave path close to the borehole in Fig. 4.12. Compare Fig. 4.3 with Fig. 4.7, it is explained by the relation between pressure of fracture fluid and arrival time of fracturing fluid. When the pumping is stopped, the variation of the travel time does not exist in Fig. 4.11(a)-(d).

4.1.2 Frequency shift analysis

Spectral centroid is a method for estimating a seismic attenuation based on frequency shift data [3]. Basic concept of this method is a comparison of spectral centroids calculated from a power spectrum

of an incident wave and a received wave. Generally, high frequency components of the propagating wave are attenuated more rapidly than low frequency components of the propagating wave in the media. Thus spectral centroid of propagating wave is downshifted during propagation in the media. In the same manner, GPR can be applied this method to estimate an electromagnetic attenuation of the media. The attenuation of GPR propagating wave is depended on the several factors. Fundamentally, the attenuation of the media is a dominant factor. However compare with seismic wave, the GPR received signal is relatively sensitive to effects of propagation and antenna radiation pattern, because these factors have a strong frequency dependency. It means that effects of propagation and antenna radiation pattern from the received signal for estimating an electromagnetic attenuation of the media should be eliminated.

At that reason, a residual spectral centroid is contrived. This method is only required a residue of two received signals and independent to effects of propagation and antenna radiation pattern. Residue of the received signals is expressed into the following equations as

$$R(f, i) = G(f)H(f, i)S(f) \quad (4-1)$$

$$R(f, i) - R(f, 0) = \Delta R(f, i) + N_0 \cong C\Delta H(f, i) + N_0 \quad (4-2)$$

where $R(f, i)$ is a spectrum of the received signal at time i , $G(f)$ includes effects of propagation and antenna radiation pattern, $H(f, i)$ is the media characteristics at time i , $S(f)$ is a spectrum of the incident signal, $\Delta R(f, i)$ is a residue spectrum of two received signals at time i , C is an attenuation coefficient, $\Delta H(f, i)$ is a variation of the media characteristics at time i , N_0 is a spectrum of noise.

Before the pressure of the fracturing fluid reaches to the breakdown pressure, the received signals are acquired in the same media characteristics. Thus residue of the received signals is only noise signal as initial in Fig. 13(a). After breakdown, the media characteristics are varied and the residual signal exists on the spectrum of noise. Its appearance is insignificantly small before the infiltrated region or the fracture contacts the propagating wave path, because only the propagating wave except the direct wave is affected by a variation of the media characteristics. When the infiltrated region contacts the propagating wave path, the residual signal appears apparently as contact in Fig. 4.13(a). In this time, a residual spectral centroid and an effective bandwidth are acquired as

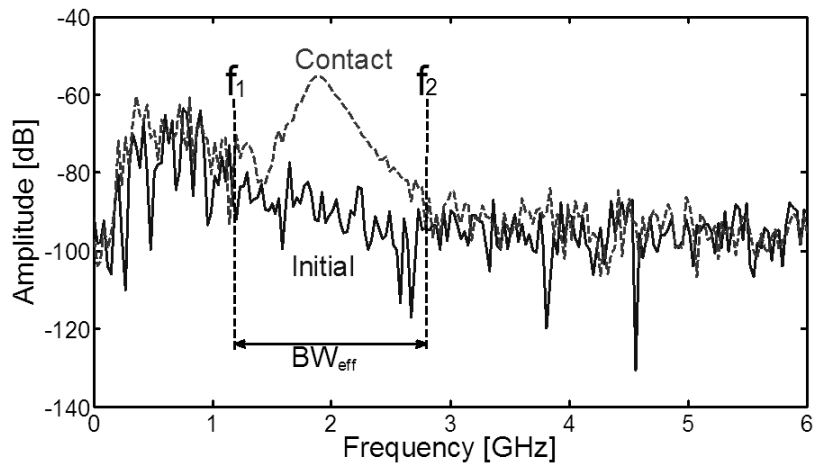
$$f_c(i) = \frac{\int_0^\infty f \Delta R(f, i) df}{\int_0^\infty \Delta R(f, i) df} = \frac{\int_{f_1}^{f_2} f \Delta R(f, i) df}{\int_{f_1}^{f_2} \Delta R(f, i) df} \quad (4-3)$$

$$BW_{eff} = f_2 - f_1 \quad (4-4)$$

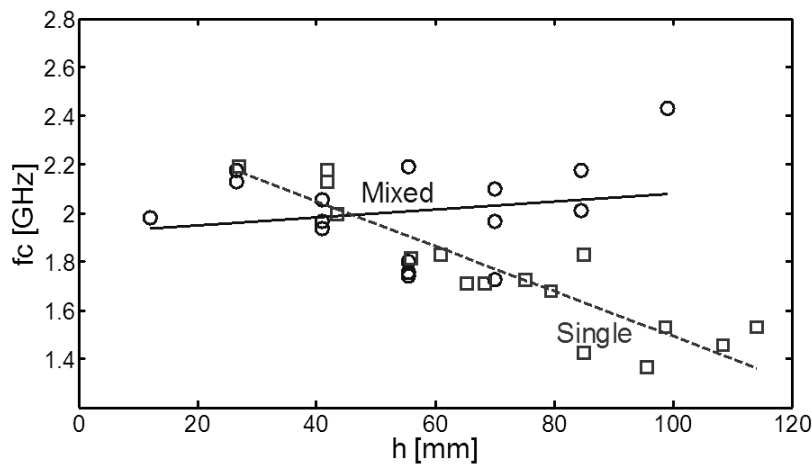
where f_c is a residual spectral centroid, BW_{eff} is an effective bandwidth.

Residual spectral centroid indicates an attenuation factor of the media related to a formation complexity of the infiltrated region. When the infiltrated region contacts the propagating wave path,

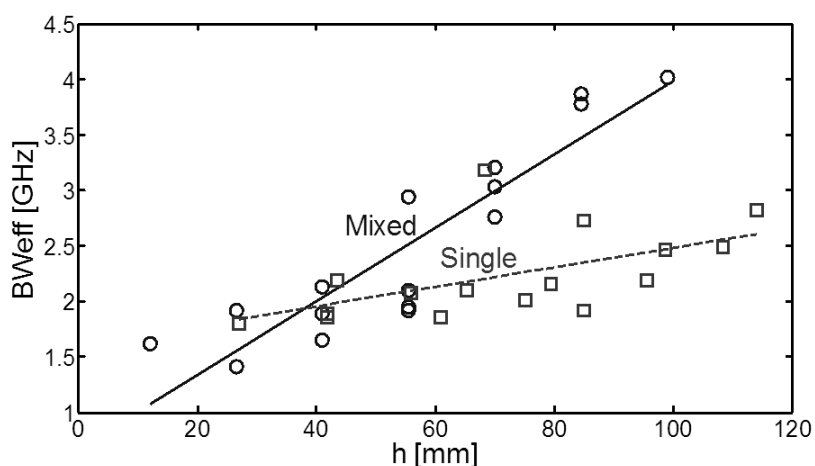
the intersection position affects to the attenuation factor of the media. Experiment with a mixed fracturing fluid has a symmetric infiltrated region, thus its residual spectral centroid is less depended on the variable h as Mixed in Fig. 4.13(b). On the other hand, experiment with single fracturing fluid has an asymmetric infiltrated region, thus its residual spectral centroid is affected by the variable h as Single in Fig. 4.13(b). Effective bandwidth represents heterogeneity of the media related to an area of the infiltrated region. Heterogeneity of the media is proportional to an expansion of the infiltrated region into the specimen. Passing through the infiltrated region, the received signal is affected by propagation factors like reflection, refraction, and diffraction. Experiment with a mixed fracturing fluid has larger the infiltrated region than experiment with a mixed fracturing fluid. In this reason, the effective bandwidth of the experiment with a mixed fracturing fluid is steeply increased as shown in Fig. 4.13(c).



(a)



(b)



(c)

Fig.4.13 Residual spectral centroid. (a) Example for explanation a concept of residual spectral centroid (b) Residual spectral centroid (c) Effective bandwidth

4.2 Monitoring of the subsurface water migration by borehole radar

Water is a fundamental substance for life conservation. Thus water activities in the atmosphere, the ocean, and the subsurface are researched to understand the environment. Especially, the subsurface water migration is closely related to agriculture. There are several measurement methods to evaluate the subsurface water migration. One of them is borehole radar which has accessibility and resolution to detect ground-water. The subsurface is expressed as water conservation system. It is approximated to LTI (Linear Time-Invariant) system. And injecting water is to be input signal of that system. Then measured travel time is set to response signal of that system. Analyzing acquired data, the subsurface characteristics like hydraulic permeability, porosity, and volumetric moisture content are acquired. Specifications of measurement are listed in Table 4.2.

Table 4.2 Specifications of measurement.

Specification	Value	Remark
Frequency	300 kHz ~ 400 MHz	Operation
Number of points	1601	-
IF bandwidth	100 Hz	-
Acquisition time	16.4 sec	A propagating wave path
Injecting rate	27.5 L/min	Fracturing fluid
Injecting time	0.25 h ~ 1.75 h	90 minutes
Area of a pit	1.62 m ²	
Distances Tx antenna to Rx antenna	2.5 m, 2.69 m	Ch.2 : 2.5 m, Ch.1 and Ch.3 : 2.69 m

4.2.1 Experiment results

Experiment is conducted two times at the same site, but different day and depth. Antennas position of 1st and 2nd experiments is shown in Fig. 4.14. Comparing these acquired data, the reproducibility of measurement and the continuity of layer will be verified.

From the electromagnetic point of view, subsurface is also a material characterized by electromagnetic parameters. Electric permittivity and permeability are representative parameters. Electric permeability will be ignored, because there are no strong ferromagnetic materials in the experiment site. On the other hand, electric permittivity divided real and imaginary parts are acquired from travel time and amplitude of received signal.

There are several methods to take travel time from received signal. One is peak amplitude time of received signal as shown in Fig. 4.15. It is easy to find out that time, if signal power level is greater than noise power level. However peak amplitude time is seriously affected by signal distortion which is occurred by heterogeneity of the subsurface. If variation of travel time is lower than fluctuating time by signal distortion, peak amplitude time does not represent travel time. Second is cross-correlation which checks a correspondence of two signals as a function of a time-lag applied to one of them. Mathematically it is expressed as

$$(f \star g)[n] = f^*[-n] \star g[n] = \sum_{m=-\infty}^{\infty} f^*[m]g[n + m] \quad (4-5)$$

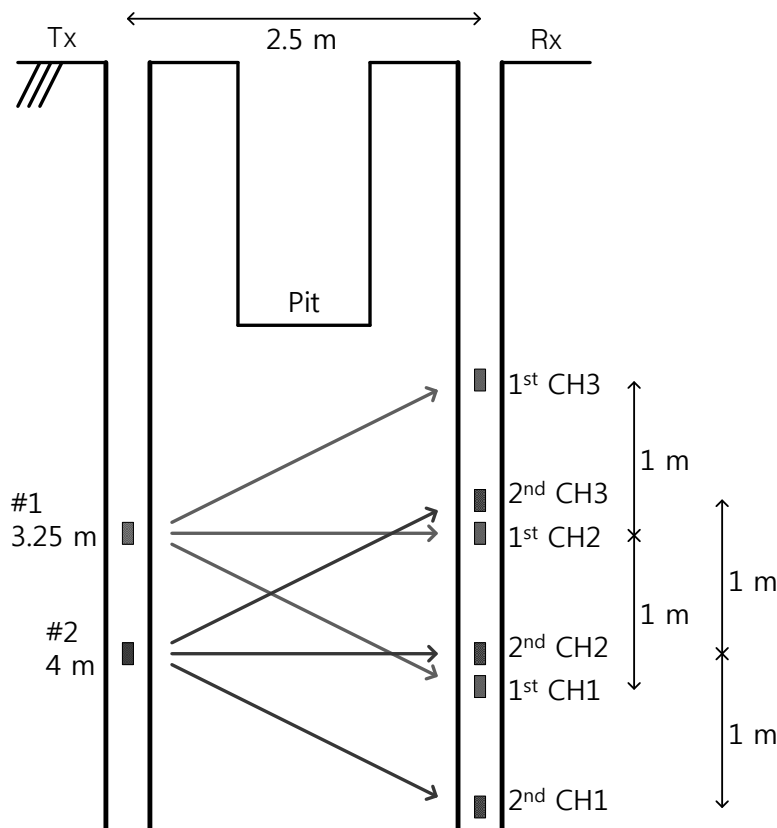


Fig.4.14 Setup of borehole radar.

Cross-correlation has maximum value when a correspondence of two signals is maximized. At that time, a time-lag n indicates a delay of two signals. However accuracy of that delay is depended on the waveform of two signals. When water infiltrated into the subsurface, received signal is dispersed and attenuated. For that result, time-lag n was fluctuated. Cross-correlation is also used to investigate an existence of secondary wave which is guided on the boundary between dry and wet layers. Unfortunately, it is difficult to detect secondary wave from received signal in this experiment, because power of secondary wave is relatively weaker than direct wave and cross-correlation resolution is poor to discriminate maximum value of cross-correlated secondary wave from a function of a time-lag. Final is leading edge of received signal as shown in Fig. 4.15. Leading edge is a detected first arrival edge which falls or rises over the noise signal level. If there is no external noise source in the subsurface, noise signal which consists of thermal noise (Natural) and internal noise (Artificial) is estimated WGN (White Gaussian Noise). First arrival edge is normally represented a part of direct wave which propagated direct path from transmitting antenna to receiving antenna. However travel time of secondary wave is smaller than travel time of direct wave under specific conditions. It is written as

$$\tau_{dir} = \frac{x\sqrt{\epsilon_{wet}}}{c} \quad (4-6)$$

$$\tau_{sec} = \frac{(x-2 \tan i_c)\sqrt{\epsilon_{dry}}}{c} + \frac{2z\sqrt{\epsilon_{wet}}}{\cos i_c c} \quad (4-7)$$

$$i_c = \sin^{-1} \left(\sqrt{\frac{\epsilon_{dry}}{\epsilon_{wet}}} \right) \quad (4-8)$$

where τ_{dir} and τ_{sec} are the travel time of direct and secondary wave, x is the distance between transmitting and receiving antenna, c is the velocity of light, i_c is the critical angle when wave propagates wet layer to dry layer, ϵ_{dry} and ϵ_{wet} are electric permittivity of dry and wet layers, z is the distance between zero-offset position to water level.

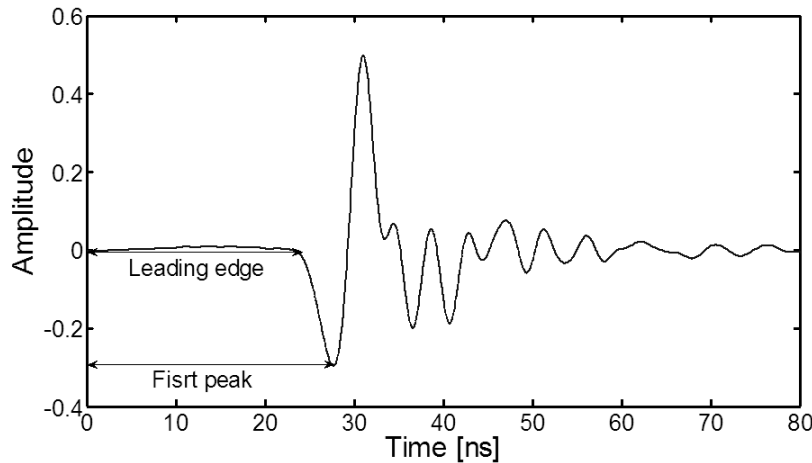


Fig.4.15 Travel times by first peak and leading edge.

However the situation ($\tau_{dir} > \tau_{sec}$) is difficult to happen, because the boundary between wet and dry layers is the irregular surface in nature. It makes to increase travel time and to reduce amplitude of secondary wave. At that reason, acquired leading edge is estimated a part of direct wave. And it is less affected distortion by heterogeneity of the subsurface. Thus leading edge method is adopted in this paper.

Ideally, amplitude of received signal is related to electrical conductivity of propagating wave path. However multipath waves generated by inhomogeneous media also affect amplitude of received signal. Thus if direct wave cannot be discriminated from received signal, acquisition of electrical conductivity of propagating wave path is difficult. On the other hand, amplitude of residual spectrum is indicated heterogeneity of the media related to an area of wet layer. Unfortunately, the experiment site is open space and inhomogeneous media, residual spectral centroid cannot be acquired.

1st experiment

From the acquired signals, leading edges of each propagating wave path are detected, but its arrival time of leading edge includes the summation of passing and processing time of measurement system. These times are acquired by zero-distance (between antennas) delay time in Table 4.3. After subtracting unnecessary time from arrival time of leading edge, it is corresponded to travel time of propagating wave path in Fig. 4.16(a). Considering with transmission distances in Table 4.2, these travel times turn to apparent permittivity in Fig. 4.16(b). It is given by

$$\varepsilon_r = \left(c \frac{T_p}{d} \right)^2 \quad (4-9)$$

where c is the velocity of light, T_p is a travel time of propagating wave, d is a distance transmitting antenna to receiving antenna.

Table 4.3 Zero-distance delay times.

Period/Channel	1 st /Ch.1	1 st /Ch.2	1 st /Ch.3	2 nd /Ch.1	2 nd /Ch.2	2 nd /Ch.3
Time [ns]	203.965	203.880	193.306	204.055	203.947	193.382

Then using Topp's equation, volumetric moisture content can be derived from apparent. Each channel has different variation start time when the infiltrated water contacts to propagating wave path, because each channel represents different subsurface layer with depth. Variation start times help to estimate vertical water infiltration velocity. Those values are given in Table. 4.4.

Table 4.4 Arrival time of the infiltrated water.

Period/Channel	1 st /Ch.1	1 st /Ch.2	1 st /Ch.3	2 nd /Ch.1	2 nd /Ch.2	2 nd /Ch.3
Time [min]	33	23	20	40	40	23

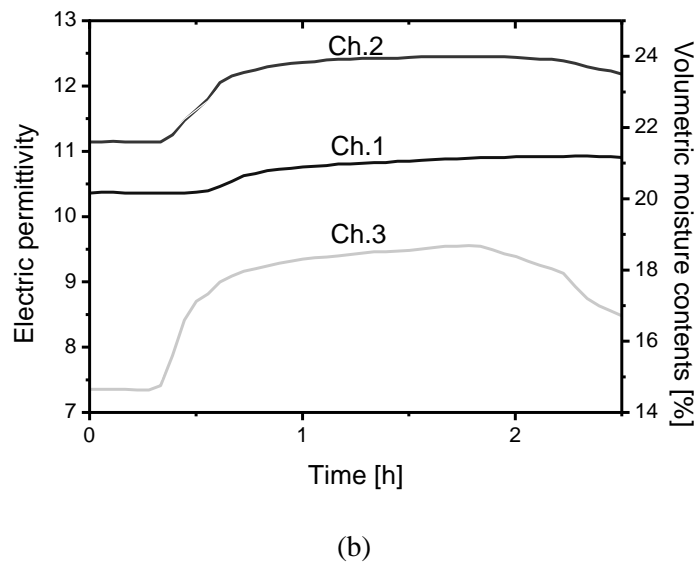
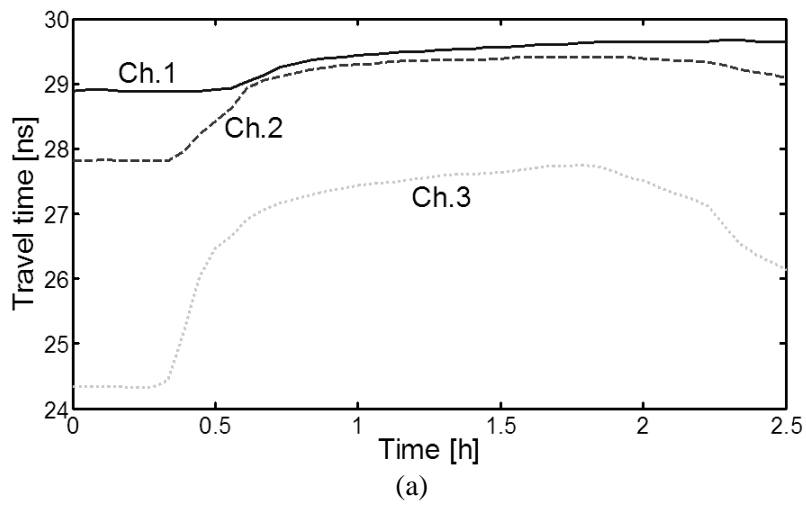


Fig.4.16 1st experiment time domain analysis
 (a) Travel time (c) Apparent permittivity.

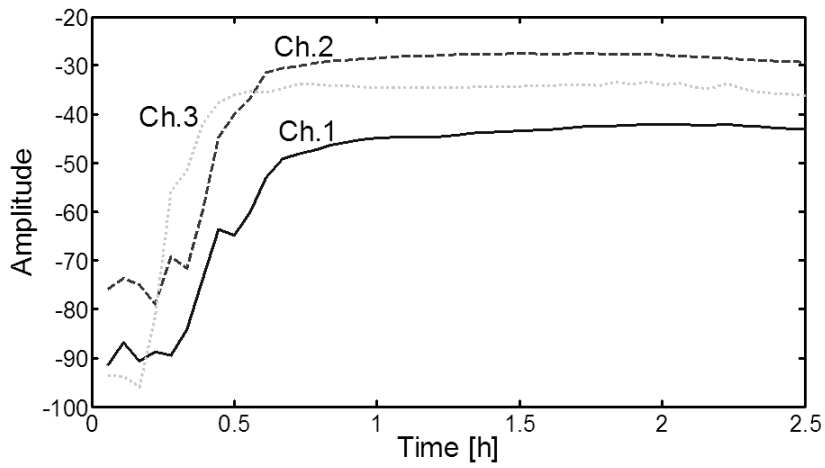
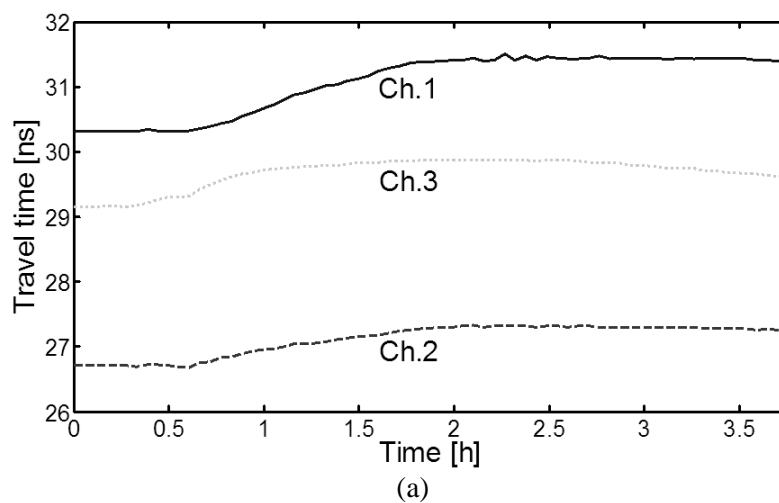


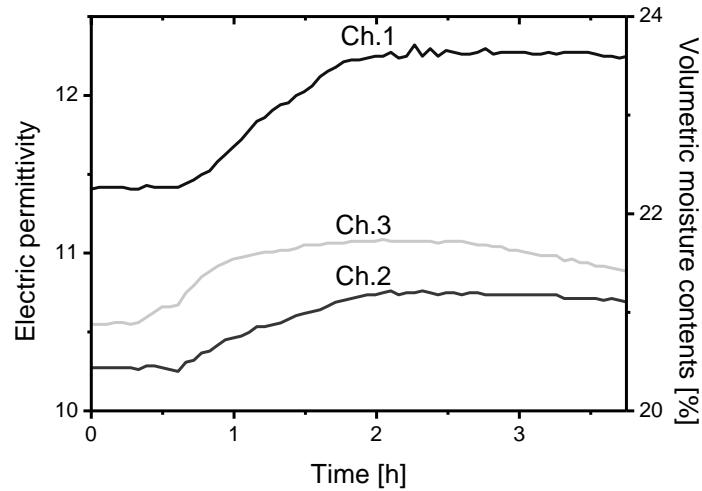
Fig.4.17 1st experiment residual variation at 225 MHz.

Although acquired residual spectrum is difficult to represent the variation in the subsurface directly, its amplitude variation tendency is connected with heterogeneity of propagating wave path. Especially, specific frequency at 225 MHz is selected to plot in Fig. 4.17, because it has enough amplitude variation. When see the variation start times, those times are earlier than previous mentioned variation start time. It means that residual spectrum at specific depth can detect a start time of precipitation or artificial water supply on the surface indirectly.

2nd experiment

From the acquired signals, leading edges of each propagating wave path are detected, and zero-distance (between antennas) delay time is acquired in Table 4.3. Then travel time of propagating wave path is calibrated in Fig. 4.18(a). Applying (4-9) and Topp's equation to calibrated times, apparent permittivity are derived in Fig. 4.18(b). Variation start times of each propagating wave path can be aligned by antenna positions. Those values are given in Table. 4.4. Comparing those results with 1st experiment results, variation degree is reduced and variation start time is increased. When water infiltrates into the subsurface, some water occupy empty pores and remain occupied place. And water infiltration proceeds to vertical and horizontal direction, infiltrated region seems to be conical shape. However 2nd experiment results are not followed upper situations. In Fig. 4.18(b), volumetric moisture content increment of channel 1 is larger than channel 2 and 3's. It means that channel 2 and 3 area have higher hydraulic conductivity than channel 1's. That result helps to explain about amplitude variation at 225 MHz plotted in Fig. 4.19. Different hydraulic conductivity means that those layers consist of different materials. And it is connected to difference of electromagnetic characteristics. Boundary between two layers is disturbed electromagnetic wave propagation, channel 1 cannot detect a start time of precipitation or artificial water supply on the surface.





(b)

Fig.4.18 2nd experiment time domain analysis

(a) Travel time (b) Apparent permittivity.

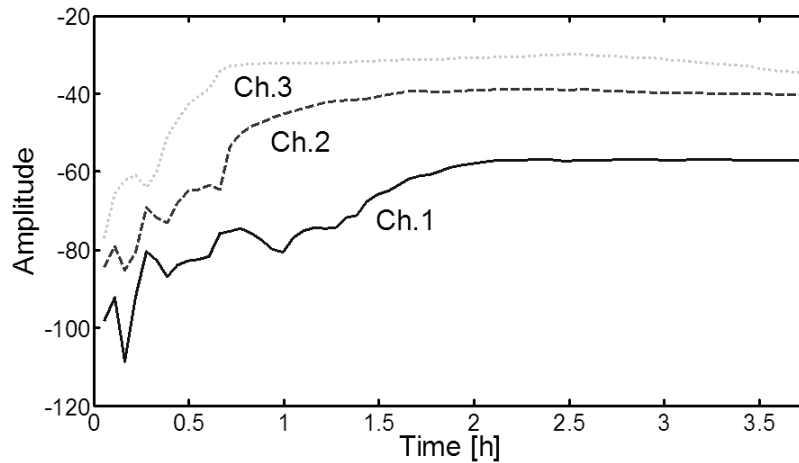


Fig.4.19 2nd experiment residual variation at 225 MHz.

4.2.2 Analysis

Comparing permittivity profiles with time acquired from data of 1st and 2nd experiments in Fig. 4.20, channel 1 of 1st experiment which represents 3.75 m depth and channel 3 of 2nd experiment which represents 3.5 m have almost same electric permittivity values. These experiments are conducted different times which are October 26th and 27th, 2010. It means that injected water at the first day is almost drained during a day. And the reproducibility of measurement and the continuity of layer are satisfied.

Analyzing a relation travel time of propagating wave path with infiltrated water, tracking method is useful. Net infiltrated the subsurface water is acquired to subtract remained water in a pit from injected water into a pit, because a thin sand layer which has low hydraulic permeability on the

surface disturbed water infiltration. Injected water is decided 27.5 L/min during 90 minutes, and contained water is calculated to multiply area of a pit by water level converted from hydrostatic pressure like meters of H₂O (mH₂O) with its temperature. Using these values, differential infiltrated water is acquired in Fig. 4.21. And explaining physical phenomenon of water infiltration in the subsurface, travel time is expressed as differential value. This value helps to quantify equilibrium water content corresponded with inflow of water indirectly. When differential infiltrated water is increased, variation of travel times is also increased in A of Fig. 4.21. Consider the positions of propagating wave path, variation start times corresponds to closeness of antenna position to the surface. However differential infiltrated water is over 25 L/min, there is no variation of travel time in B of Fig. 4.21. It means that 25 L/min inflow rate makes the subsurface passed propagating wave paths to be a quasi-saturation which is a balanced flow state in the specified area. At that reason, when inflow rate falls down under 25 L/min, quasi-saturation does not maintain. Thus variation of travel times is decreased in C of Fig. 4.21. Borehole radar can detect a quasi-saturation of transmission media through variation of travel time.

Fluid migration in porous material is followed Darcy's law as

$$q = -\frac{\vec{\kappa}}{\mu} \cdot \nabla P \quad (4-10)$$

where q is the superficial velocity, $\vec{\kappa}$ is the permeability tensor, μ is the viscosity of the interstitial fluid, ∇P is the pressure gradient.

In the experiment, the fluid viscosity μ and the pressure variation $\nabla \sigma_f$ or the volumetric flow rate Q are known parameters. Using superficial velocity q measured by the response time of each propagating wave path, the permeability tensor (Hydraulic conductivity) is derived. Basically, porosity does not affect hydraulic conductivity directly, but it affects volumetric moisture content. It means that contained water in porous material will be derived by the variation of the travel times.

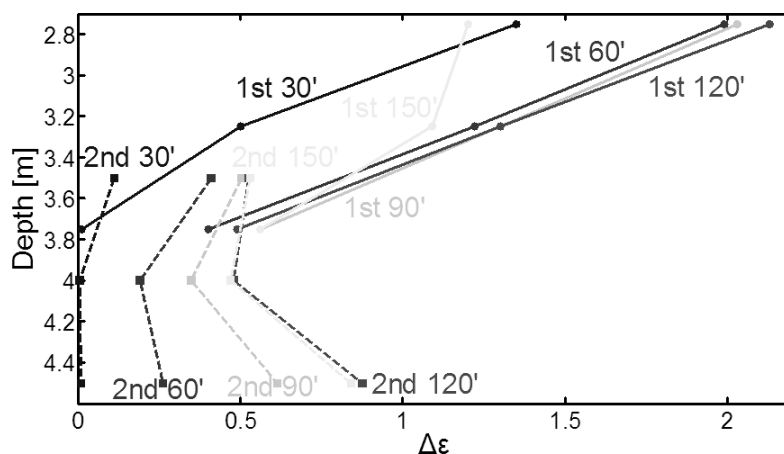


Fig.4.20 Differential permittivity profile with time.

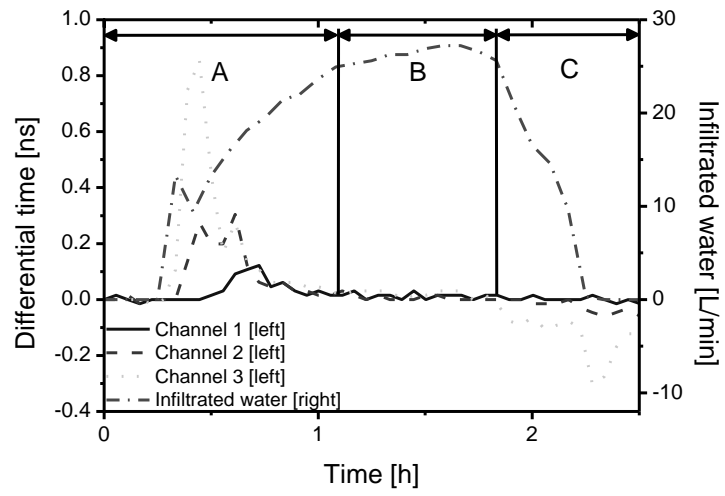


Fig.4.21 Variation of travel times with water infiltration.

Chapter 5

Fluid Migration Modeling

There are many estimation models to explain fluid migration in porous materials. Representative method is the fluid dynamics model. Using physical parameters, for example hydraulic conductivity, fluid viscosity, and porosity of material, fluid migration is estimated by computing simulation. However verification of simulation result is difficult, because fluid detection in porous material is required many sensors to flow rate and direction of fluid. And there is a possibility that these sensors disturb a flow of fluid. Meanwhile, electromagnetic model is required few parameters like electric permittivity and permeability, and electrical conductivity which are less affected by variation of temperature and pressure. Even electric permeability and electrical conductivity is vanished in the simulation, because these parameters effect to a leading edge of received signal is restricted. Verification of simulation result is conducted by comparison travel times of measurement and simulation.

5.1 Modeling of the fluid migration in a sand specimen

Specimen is an artificial object controlled materials to distribute uniformly. And fracturing fluid conserves its electromagnetic characteristics under the high pressure condition. Existence of electric permeability and electrical conductivity in simulation consumes processing time and memory without meaning. Thus simulation parameters are selected by shape data and electric permittivity.

5.1.1 1-D (Dimensional) model

When the fracturing fluid infiltrated into the specimen, the fluid invaded to not only the empty pore but also the pore which is occupied by the moisture. Hence the moisture is forced out and moves to the empty pore near the outer boundary of the region which is infiltrated by the fracturing fluid. Especially the moisture is concentrated on the direction of the growing fracture, thus the relative permittivity increases in the boundary of the infiltrated region.

To assure the above explain about the variation tendency of the travel time, a simple numerical specimen model with two regions which have different electromagnetic characteristics by sort and density of the infiltrated fluid is created, as shown in Fig. 5.1(a). The numerical specimen has a length L and contains uniformly distributed 11 % volumetric moisture content. When the fracturing fluid is infiltrated to the specimen, the specimen is differentiated into two regions. Region I is the fracturing fluid infiltrating into the specimen section, and Region II is the moisture condensed specimen section. In that time, the total moisture of whole specimen is preserved and exists in Region II. At that time,

travel time passing through whole specimen region is given as

$$V_T = V_s + V_w \quad (5-1)$$

$$\theta_{v,II} = \frac{V_w}{\frac{x}{L}V_s + V_w} \quad (5-2)$$

$$T_p = \frac{1}{c} [x\sqrt{\varepsilon_{r,I}} + (L-x)\sqrt{\varepsilon_{r,II}}] \quad (5-3)$$

where V_T , V_s , and V_w denote the total volume, the sand volume, and the water volume, respectively. $\theta_{v,X}$ is the volumetric moisture content in Region X (=I, II), x is the length in Region I. $\varepsilon_{r,X}$ is the relative permittivity in Region X. And T_p is the travel time passing through whole specimen region.

The travel times passing through whole region are changed according to the ratio between the lengths of Regions I and II and the relative permittivity in Region I as shown in Fig. 5.1(b). Compared to its constant behavior in the basis, the travel times during infiltration are changed drastically according to the fixed constant and the given variable parameters. This simulation results may help to explain the physical mechanism on the two different tendencies of the measured travel times in Fig. 4.6(a) and Fig. 4.11(a).

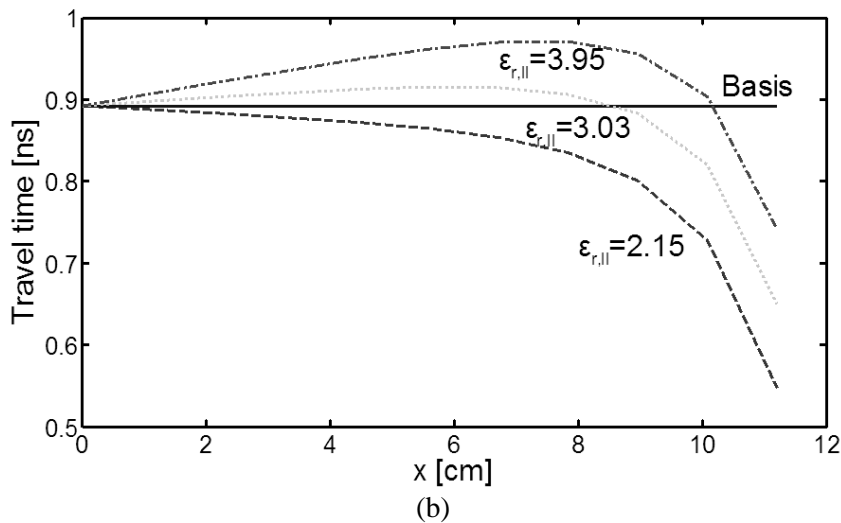
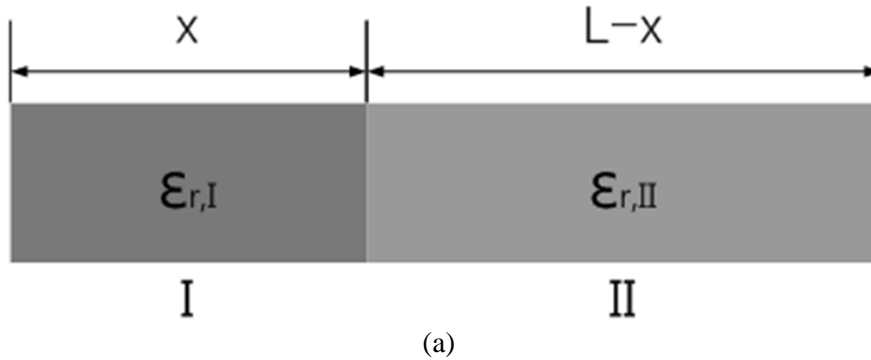


Fig.5.1 1-D model (a) 1-D migration model (b) Travel time with $\varepsilon_{r,II}$.

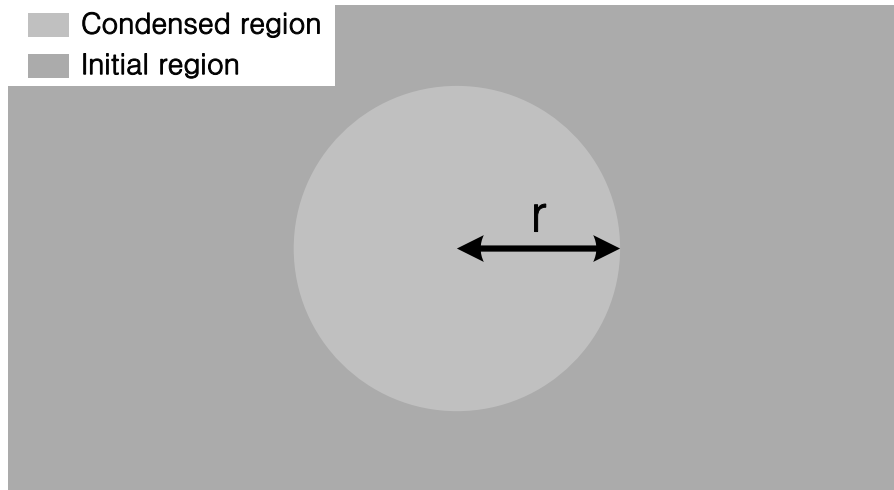
5.1.2 3-D model

Although we can possibly understand about the variation tendency of the travel time by 1-D model, it is difficult to explain fluids distribution state which indicates its density of specified region in the specimen. There are several methods for measuring volumetric moisture content. One of them is TDR. However a required measurement area of TDR probe is larger than specified region in the specimen, precise moisture distribution state in the specimen cannot be acquired. In this reason, a forwarding model using FDTD (Finite Difference Time Domain) simulation is designed and conducted.

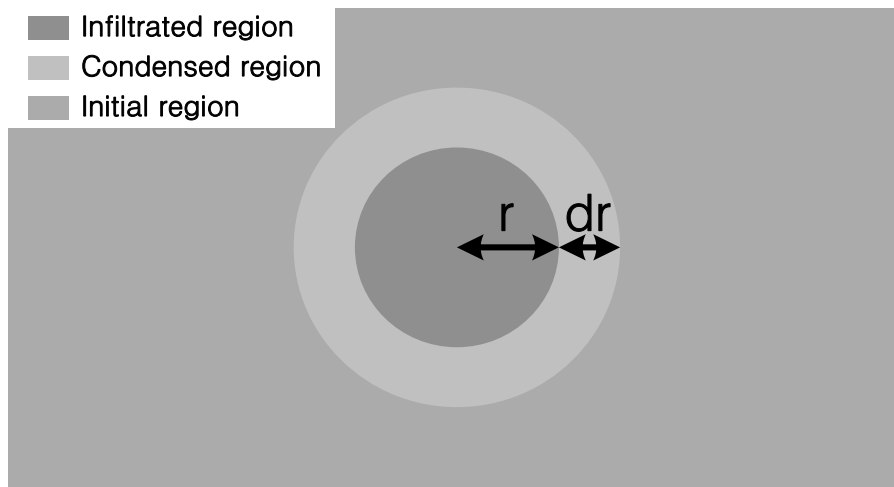
A physical situation of the specimen must be considered, before design a FDTD model. Specimen is blocked by metal plates and compressed by hand pumps. Thus a volume and the moisture content of the specimen are preserved even fracturing fluid is infiltrated into the specimen. Colligating these factors, the moisture in the infiltrated region is forced out and moved the condensed region by a pressured fracturing fluid. Three hypotheses based on the distribution of the condensed region in the specimen are suggested. At first, the condensed region is set to whole specimen except the infiltrated region as shown in Fig. 5.2(a). At second, the condensed region is positioned to boundary between the infiltrated region and the initial region which is not affected by the infiltration in Fig. 5.2(b). And it has a constant width. At third, the definition of the condensed region is almost same to second, however a width of the condensed region is proportional to a volume of the infiltrated region. Volumetric moisture content in the condensed region of each hypothesis is numerically expressed as (A.1).

After conducting FDTD simulation, those results are compared with the experiment result. Simulation result tendency of hypothesis III in Fig. 5.3(c) is well matched to experiment result in Fig. 4.6(a). It means that the infiltrated region is discriminated the infiltrated region filled with the fracturing fluids and the condensed region filled with the moisture before regarded as same infiltrated regions divided by fracturing fluids have different viscosity as shown in Fig. 4.4. When the fracturing fluid infiltrated into a specimen, first arriving fluid migrated region is the condensed region. A travel time corresponded to its propagating wave path is delayed when the condensed region passes through a propagating wave path, because the relative permittivity of the condensed region is greater than the relative permittivity of the initial region. After that, the infiltrated region also reaches to a propagating wave path. At that time, an increment of a travel time is changed, because the relative permittivity of the infiltrated region is lower than the relative permittivity of the initial region. Imbalance expansion of fluid migrated regions is also affected an increment of a travel time. Total injected fracturing fluid into a specimen is continuously increased. On the other hand, total moisture in a specimen is maintained. Thus a volume increment of the infiltrated region is greater than a volume increment of the condensed region. It means that an effect of the infiltrated region to a travel time is more effective than an effect of the condensed region to a travel time. For that reason, each propagating wave paths are corresponded to different travel time variations.

Fluids distribution of hypothesis III is also explained a physical restriction of fluid migration in the specimen. When the moisture is moved to the condensed region, it is compressed and saturated with 28 % of the specimen volume. Because the porosity of the specimen is around 28 % that means only 28 % of the specimen volume is occupied by air, fracturing fluid, or moisture.



(a)



(b)

Fig.5.2 3-D model (a) Hypothesis I (b) Hypothesis II and III.

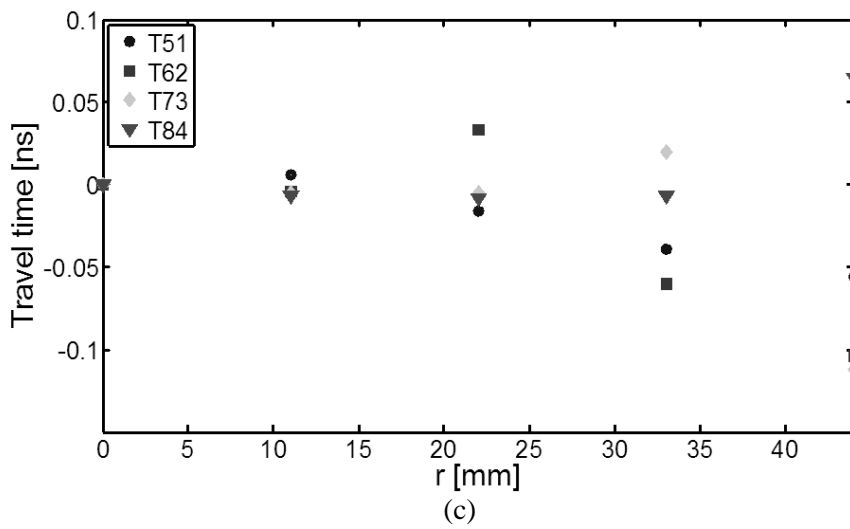
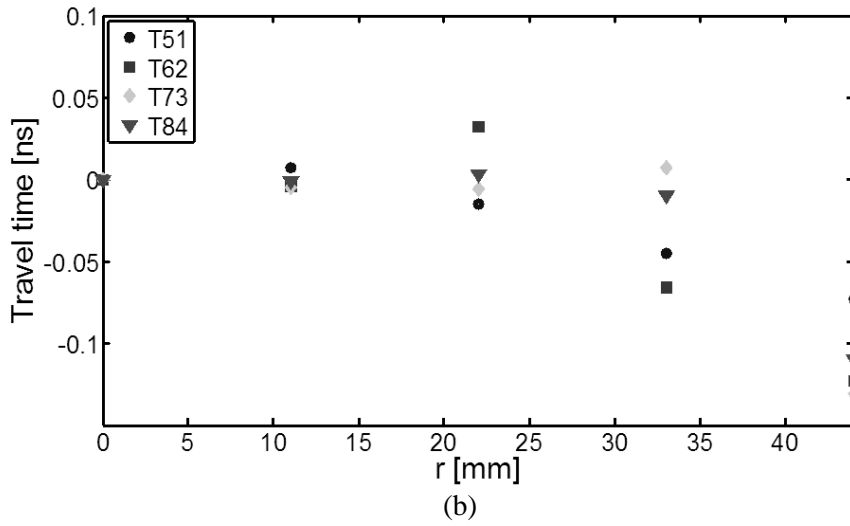
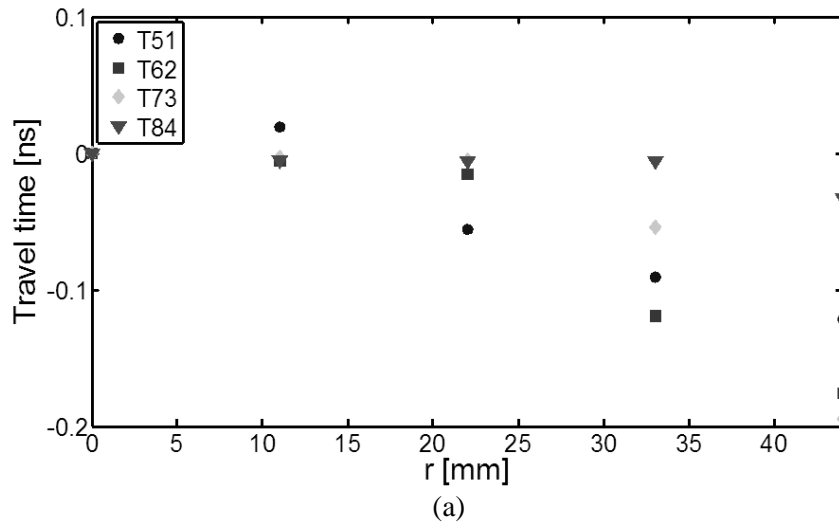


Fig.5.3 FDTD results (a) Hypothesis I (b) Hypothesis II (c) Hypothesis III.

5.1.3 Analysis

There are three phases which are water, air, and fracturing fluid in a specimen. Fluid migration in a specimen indicates that variation of fluid movement and distribution by fluid dynamics and chemical reactions between these phases. Small droplets of fracturing fluid invade into air occupied pores of specimen by pressure of fracturing fluid. Air in an infiltrated region is pushed out of its own position, and then compressed to neighbor air occupied pores. In high pressure state, some compositions of air, especially oxygen, are easily dissolved in water. For that reason, air migration from an infiltrated region to another region is less effect to a material distribution in a specimen. Water occupied pores are also invaded by fracturing fluid. Water droplets in an infiltrated region are migrated to pores in another region. At that time, water does not mix with fracturing fluid, and a volume of water is almost same even in high pressure state. Thus water migration from an infiltrated region to another region is quietly affected a material distribution in a specimen.

5.2 Modeling of the subsurface water migration

5.2.1 Piston model without edge leakage effect

Piston model approximates that fluid migration formation is a rectangle shape and moves to straight down as shown in Fig. 5.4. At that time, subsurface is designed as homogeneous media which has same electric permittivity, but has different hydraulic conductivity with depth. Water infiltrated region has electric permittivity which is larger than subsurface's value. Thus variation of travel time of each propagating wave path is affected by position (Depth) and movement velocity of water front. Relation between travel time and depth of water front is expressed as

$$T_p = \frac{1}{c} [\sqrt{\varepsilon_{r,I}}(L - d \cdot \operatorname{cosec}(\theta)) + \sqrt{\varepsilon_{r,II}}d \cdot \operatorname{cosec}(\theta)] \quad (5-7)$$

$$d \cdot \operatorname{cosec}(\theta) \leq L \quad (5-8)$$

where d is the depth of water front, c is the velocity of light, $\varepsilon_{r,I}$ is the electric permittivity of initial region, L is the length of propagating wave path, θ is the incline angle of propagating wave path, $\varepsilon_{r,II}$ is the electric permittivity of infiltrated region.

Deriving the depth of water front d from given equations, electric permittivity of each region must be decided. However electric permittivity of initial and quasi-saturation state with depth is different as shown in Fig. 4.16(b) and 4.18(b). At that reason, fluctuation of electric permittivity is normalized which initial and quasi-saturation state are set 0 and 1 in Fig. 5.5. The depth of water front d is calculated by (5-7) and (5-8) with experiment data. At that time, channel 2 is assumed to have the incline angle of propagating wave path, because its d value is expressed as step function in the calculation. Using these values, the movement velocity of water front is derived as

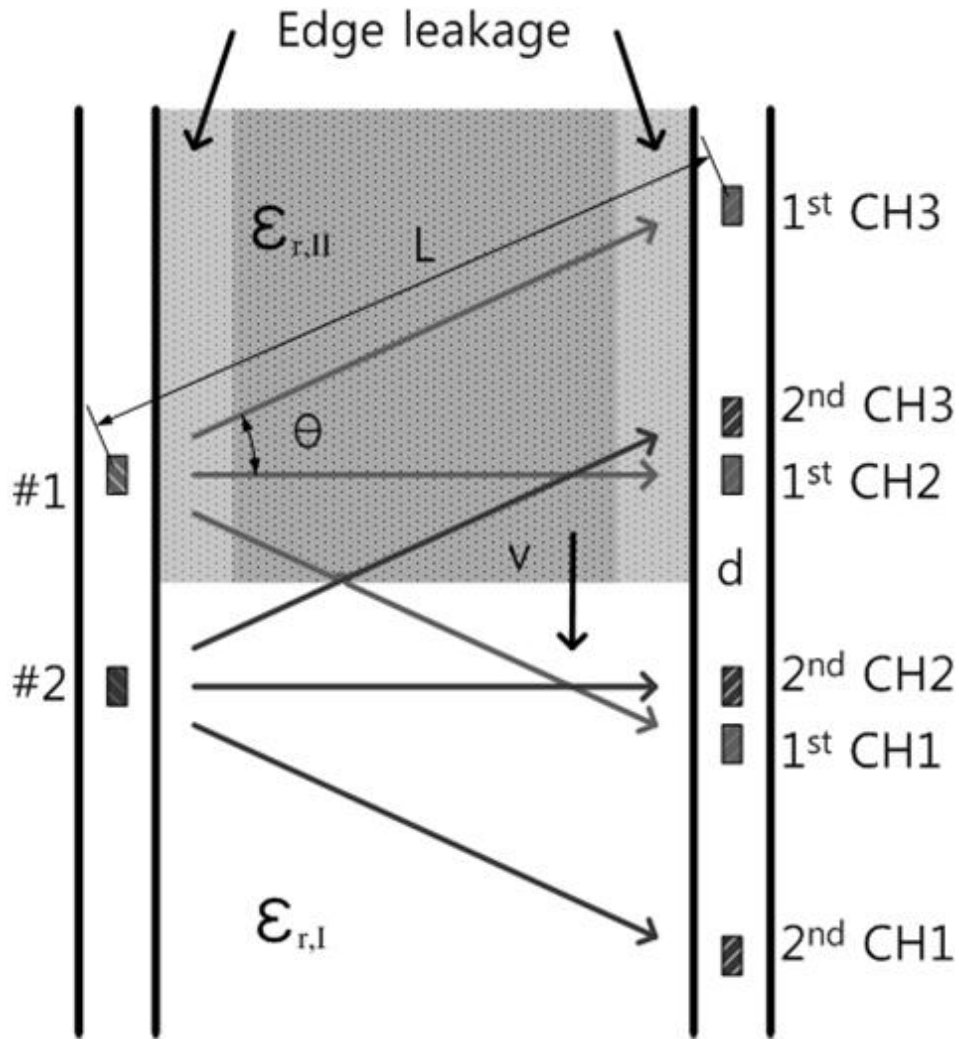


Fig.5.4 Effect of water front movement to travel time.

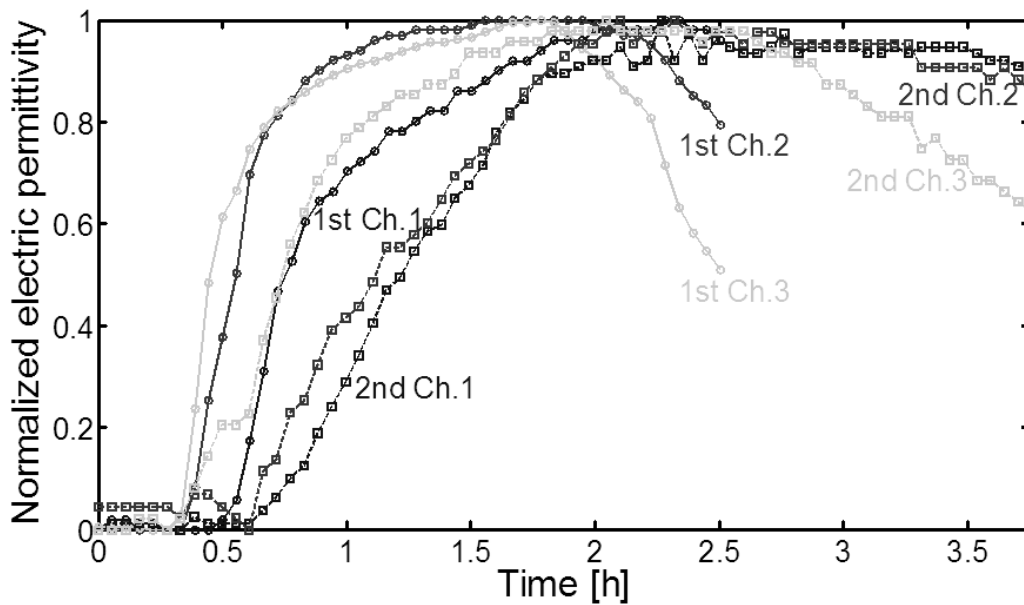


Fig.5.5 Normalized fluctuation of electric permittivity.

$$v_{water}(\tau) = \frac{d}{d\tau} d(\tau) \quad (5-9)$$

where τ is the actual time.

Then mean, variance, and peak values are listed in Table 5.1. These values indicate that infiltration velocity is getting reduced when water front moves to down.

However results of this model break a fundamental rule which electric permittivity of infiltrated region is not changed. Infiltration velocity of channel 3 is still increased even after infiltration velocity of channel 1 is getting increased. Thus this phenomenon should be explained by physical infiltration mechanism.

Table 5.1 Mean and variance values of infiltration velocity.

Period/Channel	1 st /CH.1	1 st /Ch.2	1 st /Ch.3	2 nd /CH.1	2 nd /Ch.2	2 nd /Ch.3
Peak [m/h]	2.81	3.476	4.418	1.1716	2.082	2.626
Mean [m/h]	0.8214	1.791	1.408	0.7536	0.7606	0.7738
Variance [m/h ²]	0.3532	0.638	1.078	0.0444	0.1272	0.2388

5.2.2 Piston model with edge leakage effect

In nature, water does not infiltrate only down direction, but also side direction. It is happened by water itself gravity and osmotic pressure. Thus there is unstable variation around the last saturating stage. Considering stable fluctuation state within 0.7 of normalized value, d is calculated by (5-7) and (5-8) with experiment data. And the movement velocity of water front is derived by (5-9). Then mean, variance, and peak values are listed in Table 5.2. At that time, envelop infiltration velocity is acquired by selecting maximum value of each time in Fig. 5.6.

Comparing boreholes distance (2.5 m) and pit width (0.9 m), infiltrated region affects a part of propagating wave path calculated by ratio between boreholes distance and pit width. Water front depth is expressed in Fig. 5.6.

Table 5.2 Mean and variance values of infiltration velocity.

Period/Channel	1 st /CH.1	1 st /Ch.2	1 st /Ch.3	2 nd /CH.1	2 nd /Ch.2	2 nd /Ch.3
Peak [m/h]	2.81	3.054	4.418	1.1578	2.082	2.626
Mean [m/h]	2.1024	2.5056	4.0816	0.807	0.8726	1.2336
Variance [m/h ²]	0.2858	0.1126	0.1134	0.0458	0.1972	0.3938

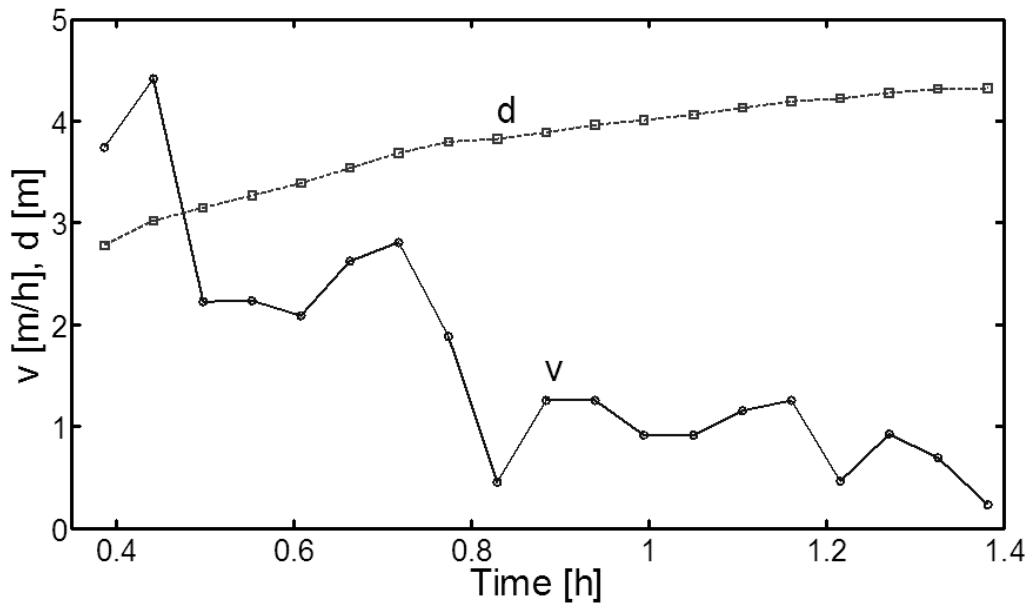


Fig.5.6 Envelop infiltration velocity and water front depth.

Chapter 6

Conclusions

The research works are conducted to develop radar technologies to monitoring fluid migration in porous material. Two different radar systems are designed to measure electromagnetic field generated by environmental variation. The most part of the text of contents from chapter 2 to chapter 5 are spent on experiment, modeling, and analysis about GPR measurement to monitoring fluid migration in the unconsolidated rock and Borehole radar measurement to monitoring the subsurface water migration. Main issues of the text of contents are divided into three sections. What are the characteristics of porous materials and fluids? How acquire significant radar signals by fluid migration in porous material? How derive fluid migration mechanism in porous material from the migration model estimated by measurement and simulation data? Following summary of each chapter deals with main issues.

In chapter 2, expected fluid migration phenomena under given environmental conditions are presented. The unconsolidated sand and the fracturing fluid are selected to extract methane hydrate using hydraulic fracturing in the reservoir. The fracturing fluid is injected gradually into borehole inserted into the reservoir. Under the certain pressure defined by hydraulic conductivity of the reservoir, the fracture fluid cannot infiltrate into the reservoir. When breakdown is happened, fracture is generated and extended with certain direction determined by tectonic stresses. At that time, fluid migration is appeared to infiltrate into the reservoir through fracture corridor by physical and chemical relations among three phases which are fracturing fluid, water, and air. When fracturing fluid pressure below tectonic stresses, fracture generating is stopped and fracture corridor is closed. Thus fluid migration is halted. In the same manner, surface water is infiltrated into the subsurface by its gravity and osmosis pressure. Comparing fluid migration in the unconsolidated sand, the subsurface is inhomogeneous media and tectonic stresses can be ignored. Thus the subsurface water migration is shown irregular movement and distribution.

In chapter 3, necessities of radar applications to monitoring fluid migration in porous material are presented by characteristics of materials and measurement configurations. The specimen is the unconsolidated sand produced to conduct preliminary experiment of hydraulic fracturing for evaluating extraction of methane hydrate. Thus conventional geophysics techniques which are applied resource exploration are difficult to measure fluid migration in the unconsolidated sand. However radar technique can acquire significant signal using electromagnetic wave less affected by material physical states. Electric permittivity difference between the specimen and the fracturing fluid is a dominant variation cause of wave propagation velocity derived from measured travel time and

propagation path length in media. Fracture is detected indirectly by monitoring of infiltrated region expansion, because fracture width is too small to measure using radar even open state. Measurement system is adopted VNA which has high dynamic range and Vivaldi array antennas which have wide bandwidth. Those measurement characteristics help to acquire precise travel time and high spatial resolution of received signal. Borehole radar system is conducted the same operation as previous one to measure the subsurface water migration, however it is concentrated on the suppression of mutual coupling and noise effect. For that purpose, optical link system and narrow IF bandwidth are adopted. Comparing previous one, those make long measurement setup time and data acquisition time. However, even which infiltration velocity is faster than natural state why injection rate is abnormally high, data acquisition time is enough to trace it.

In chapter 4, analyses of measured data in the time and the frequency domains using several signal processing techniques are presented. Basically, most important data to monitoring fluid migration in porous material is travel time of received signal. There are several methods to detect a time delay corresponded to travel time. One of them is the leading edge method which is strong to the background noise and signal dispersion. Using that method, infiltration velocity is acquired by response times of each propagating wave path. Experiment results of fluid migration in the unconsolidated sand are shown that the variation of the travel time of each propagating wave path are divided into decrement tendency expected phenomenon and increment tendency unexpected phenomenon. Those phenomena are required new fluid migration model which is multi-phase model, not two-phase model. Effects of the fracturing fluid viscosity to pressure of breakdown, infiltration velocity, and spreading of the infiltrated region are explained. Experiment results of the subsurface water migration are shown that the subsurface is inhomogeneous and continuous media, and the borehole radar with optical link system has the reproducibility. Quasi-saturation and equilibrium moisture contents of the subsurface are acquired by net infiltrated the subsurface water and measured travel times. In the frequency domain analysis, concepts of residual centroid frequency and effective bandwidth are suggested to explain the symmetry and the heterogeneity of infiltrated region. These concepts are new signal processing approaches to monitoring fluid migration in porous material.

In chapter 5, numerical and simulation results of suggested models to explain physical phenomena is presented. Forwarding model of fluid migration is assumed that contained water in a specimen affects travel time of each propagating wave path. Based on that assumption, numerical 1-D model is designed by expected parameters and shown variation of travel time with the expansion of the infiltrated region in mass conservation state. Considering fluid dynamics and tectonics, FDTD 3-D models are designed. And simulation parameters which size and electric permittivity of a specimen and the infiltrated region are selected by suggested hypotheses. Comparing simulation results with experiment result, water saturation hypothesis can explain the variation tendency of the travel time during fluid migration. And 2-D tomography helps the analyst to understand fluid migration in a

specimen visually. Piston model is suggested to explain the subsurface water migration. It is simple model restricted the infiltrated region within a vertically extended block, thus many parameters are approximated and ignored. Also number of acquired signal is restricted by fixed antenna position and limited measurement time, even cannot make a tomography. Although these conditions, hydraulic conductivity derived from infiltration velocity. In summary of this thesis, the author contrives monitoring of fluid migration in the unconsolidated sand and the subsurface water migration. Experiments and its preparations are conducted to acquire significant data. Then acquire data are analyzed by several signal processing. At that time, new frequency shift analysis which concepts of residual centroid frequency and effective bandwidth are suggested. Finally, migration models are designed and proven by FDTD and piston model.

Outgrowth of this thesis will be helpful for enhancing the exploitation technique of the methane hydrate and the investigation of ground water. Moreover not only mentioned applications, the exploitation of other natural resource, the development of geothermal power generation, and the preparation for preventing natural disasters are also applied.

Appendix

A.1 Volumetric moisture content in the condensed region

Volumetric moisture content in the condensed region of each hypothesis are expressed into following equations

$$\theta_v = \frac{V_w}{\frac{V_{con}}{V_{inf} + V_{con}} V_s + V_w} \cong \frac{V_w}{V_s + V_w} \quad (A-1)$$

$$\theta_v = \frac{V_w}{\frac{V_{con}}{V_{inf} + V_{con}} V_s + V_w} = \frac{V_w}{\frac{\left(k \frac{2(r+dr)^3}{3} + \frac{2(r+dr)^3}{3}\right) - \left(k \frac{2r^3}{3} + \frac{2r^3}{3}\right)}{k \frac{2(r+dr)^3}{3} + \frac{2(r+dr)^3}{3}} V_s + V_w} = \frac{V_w}{\left(1 - \frac{1}{\left(1 + \frac{dr}{r}\right)^3}\right) V_s + V_w} \quad (A-2)$$

$$\theta_v = \frac{V_w}{\frac{V_{con}}{V_{inf} + V_{con}} V_s + V_w} = \frac{V_w}{\frac{\left(k \frac{2(r+cr)^3}{3} + \frac{2(r+cr)^3}{3}\right) - \left(k \frac{2r^3}{3} + \frac{2r^3}{3}\right)}{k \frac{2(r+cr)^3}{3} + \frac{2(r+cr)^3}{3}} V_s + V_w} = \frac{V_w}{\left(1 - \frac{1}{(1+c)^3}\right) V_s + V_w} \quad (A-3)$$

where V_w and V_s denote the water volume and the sand volume, V_{inf} and V_{con} denote the volume of the infiltrated region and the volume of the condensed region, respectively. k is a coefficient of an infiltration intensity. c is a ratio between a thickness of the condensed region and a radius of the infiltrated region.

In hypothesis I, a volume of the infiltrated region is relatively small than a volume of whole specimen. Thus volumetric moisture content in the condensed region is approximated to an initial value. In hypothesis II, volumetric moisture content in the condensed region is depended on a volume of the infiltrated region. Thus it is proportional to a volume of the infiltrated region. In hypothesis III, volumetric moisture content in the condensed region is independent of a volume of the infiltrated region. Thus it has a constant value.

A.2 2-D tomography

Number of propagating wave paths is sixteen in the hydraulic fracturing experiment. Thus maximum cell number to express the variation of area characteristics by tomography is also sixteen. Cross-section of specimen around the infiltrated region can be divided as shown in Fig. A.1. And electric permittivity of each area with time is given as

$$[T(t)] = [C][A(t)] \quad (A-4)$$

$$[A(t)] = [C]^{-1}[T(t)] \quad (A-5)$$

$$A_{\varepsilon_r} = \left(\frac{cA}{d}\right)^2 \quad (A-6)$$

where T is 16 by 1 measured travel time matrix, C is 16 by 16 coefficient matrix which each element value is normalized length of propagating wave path in each cell area, A is 16 by 1 area

characteristic matrix which each element value is time to pass through each cell area, t is an experiment time, c is the velocity of light, d is the unit distance, A_{ε_r} is the electric permittivity of cell area.

Coefficient matrix C is a singular matrix, normal inverse matrix method is not converted coefficient matrix C to inverse coefficient matrix C^{-1} . However using pseudo-inverse matrix method, it is possible to acquire inverse coefficient matrix C . Then electric permittivity of each cell area with time is acquired. It is able to discriminate between infiltrated region and condensed regions. Also real-time fluid migration image expressed by 2-D tomography will help to analyze hydraulic fracturing mechanism.

Deriving area characteristic matrix A from acquired travel time vector, travel time of each propagating wave path should be defined as

1st routes

$$\begin{bmatrix} T_{S51}(t) \\ T_{S62}(t) \\ T_{S73}(t) \\ T_{S84}(t) \end{bmatrix} = \begin{bmatrix} A_{11}(t) + A_{21}(t) + A_{31}(t) + A_{41}(t) \\ A_{12}(t) + A_{22}(t) + A_{32}(t) + A_{42}(t) \\ A_{13}(t) + A_{23}(t) + A_{33}(t) + A_{43}(t) \\ A_{14}(t) + A_{24}(t) + A_{34}(t) + A_{44}(t) \end{bmatrix} \quad (\text{A-4})$$

2nd routes

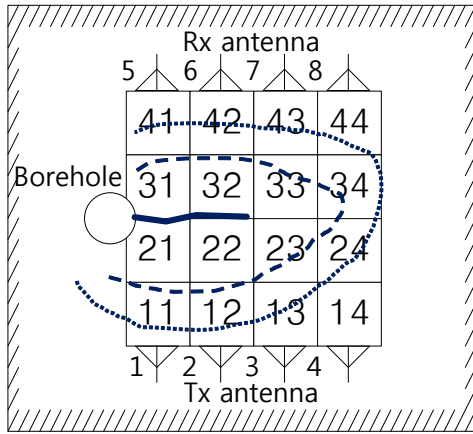
$$\begin{bmatrix} T_{S61}(t) \\ T_{S52}(t) \\ T_{S72}(t) \\ T_{S63}(t) \\ T_{S83}(t) \\ T_{S74}(t) \end{bmatrix} = \frac{\sqrt{17}}{4} \begin{bmatrix} A_{11}(t) + A_{21}(t) + A_{32}(t) + A_{42}(t) \\ A_{12}(t) + A_{22}(t) + A_{31}(t) + A_{41}(t) \\ A_{12}(t) + A_{22}(t) + A_{33}(t) + A_{43}(t) \\ A_{13}(t) + A_{23}(t) + A_{32}(t) + A_{42}(t) \\ A_{13}(t) + A_{23}(t) + A_{34}(t) + A_{44}(t) \\ A_{14}(t) + A_{24}(t) + A_{33}(t) + A_{43}(t) \end{bmatrix} \quad (\text{A-5})$$

3rd routes

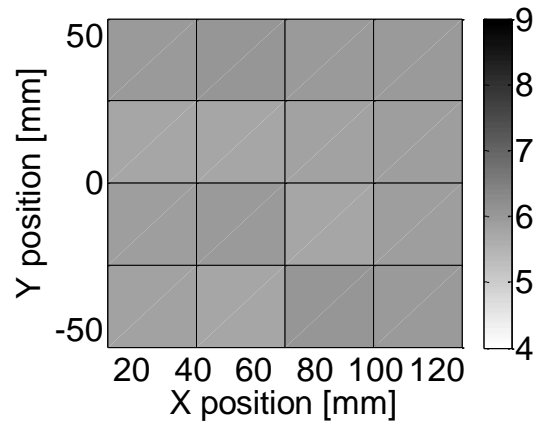
$$\begin{bmatrix} T_{S71}(t) \\ T_{S53}(t) \\ T_{S82}(t) \\ T_{S53}(t) \end{bmatrix} = \frac{\sqrt{20}}{4} \begin{bmatrix} A_{11}(t) + A_{22}(t) + A_{32}(t) + A_{43}(t) \\ A_{13}(t) + A_{22}(t) + A_{32}(t) + A_{41}(t) \\ A_{12}(t) + A_{23}(t) + A_{33}(t) + A_{44}(t) \\ A_{14}(t) + A_{23}(t) + A_{33}(t) + A_{42}(t) \end{bmatrix} \quad (\text{A-6})$$

4th routes

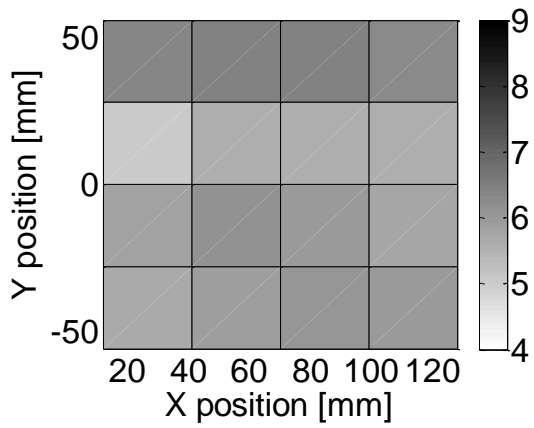
$$\begin{bmatrix} T_{S81}(t) \\ T_{S54}(t) \end{bmatrix} = \frac{5}{4} \begin{bmatrix} \frac{2}{3}A_{11}(t) + \frac{1}{3}A_{12}(t) + A_{22}(t) + \frac{2}{3}A_{33}(t) + \frac{1}{3}A_{43}(t) + A_{44}(t) \\ \frac{2}{3}A_{14}(t) + \frac{1}{3}A_{13}(t) + A_{23}(t) + \frac{2}{3}A_{32}(t) + \frac{1}{3}A_{42}(t) + A_{41}(t) \end{bmatrix} \quad (\text{A-7})$$



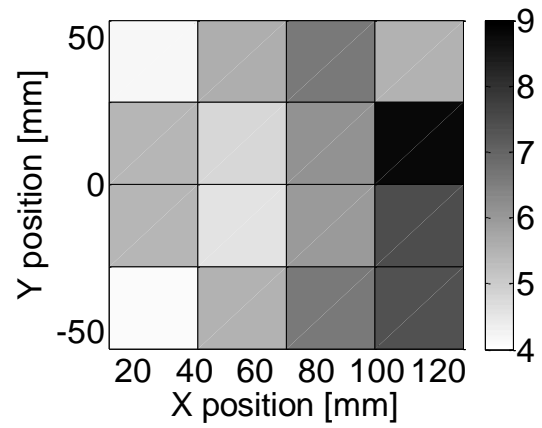
(a)



(b)



(c)



(d)

Fig.A.1 2-D electric permittivity tomography

(a) Mapping (b) Initial (0 min) (c) After breakdown (3 min) (d) Final (15 min).

References

- [1] B. Bohloli, C. J. de Pater, "Experimental study on hydraulic fracturing of soft rocks: influence of fluid rheology and confining stress," *Journal of Petroleum Science and Engineering*, 53(1-2):1-12, 2006.
- [2] U.S. Geological Survey, <http://www.usgs.gov/>
- [3] T. Takayama, M. Sato, "A Novel Direction-Finding Algorithm for Directional Borehole Radar," *IEEE Trans. Geosci. Remote Sensing*, vol. 45, issue 8, pp. 2520-2528, Aug. 2007.
- [4] Research Consortium for Methane Hydrate Resources in Japan, <http://www.mh21japan.gr.jp/>
- [5] R. Helmig, *Multiphase Flow and Transport Processes in the Subsurface: A Contribution to the Modeling of Hydrosystems*, Springer Verlag, Berlin, 1997.
- [6] J. Bear, *Dynamics of Fluids in Porous Media*, Dover Publications, 1972.
- [7] G. C. Topp, J. L. Davis, and A. P. Annan, "Electromagnetic determination of soil water content: Measurement in coaxial transmission lines," *Water Resour. Res.*, vol. 16, pp. 574-582, 1980.
- [8] Y. Yang, C. Zhang, S. Lin, and A. E. Fathy, "Development of an ultra wideband Vivaldi antenna array," *IEEE AP-S International Symposium on Antennas and Propagation*, 3-8 Jul. 2005, vol. 1A, pp. 606-609.
- [9] S.G. Kim and K. Chang, "Ultra wideband exponentially-tapered antipodal Vivaldi antennas," in *IEEE AP-S International Symposium on Antennas and Propagation*, Jun. 2004, vol. 3, pp. 2273-2276.
- [10] J. P. Weem and Z. Popovic, "Vivaldi antenna arrays for SKA," in *Proc. Antennas and Propagation Soc. Int. Symp.*, 2000, vol. 1, pp. 174-177.
- [11] S. Kuroda and T. Shibuya, "Cross borehole radar monitoring for the vadose zone process beneath an artificial pond," *122th Society of Exploration Geophysicists of Japan Conference*, 2010, pp. 296-297.

- [12] D. F. Rucker and Ty P. A. Ferre, "Parameter Estimation for Soil Hydraulic Properties Using Zero Offset Borehole Radar: Analytical Method," *Soil Sci. Soc. Am. J.*, pp.1560-1567, 68, 2004.
- [13] A. Igarashi, T. Ito, K. Yamamoto, S. Nagakubo, and K. Suzuki, "Laboratory Study of Hydraulic Fracturing Behavior in Unconsolidated Sands for Methane Hydrate Production," *Offshore Technology Conference*, Houston, Texas, USA, 5-8 May 2008, 19324-MS.
- [14] C. J. de Pater and Y. Dong, "Experimental study of hydraulic fracturing sand as a function of stress and fluid rheology," SPE 105620, *Proc. 2007 SPE Hydraulic Fracturing Conference*, College Station, Texas, USA, Jan. 2007, pp. 29-31.
- [15] Y. Quan, and J. M. Harris, "Seismic attenuation tomography using the frequency shift method," *Geophysics*, 62, pp. 895-905, 1997.
- [16] T. Miwa, M. Sato, and H. Niitsuma, "Subsurface fracture measurement with polarimetric borehole radar," *IEEE Trans. Geosci. Remote Sensing*, pp.828-837, vol.37, no.2, 1999.
- [17] Miwa, T., Sato, M., "Polarimetric Borehole Radar System for Fracture Measurement," *Subsurface Sensing Technologies and Applications*, pp.161-175, vol.1, no.1, 2000.
- [18] M. W. Whitt, F. T. Ulaby, P. Polatin, and V. V. Liepa, "A general polarimetric radar calibration technique," *IEEE Trans. Antennas Propag.*, pp.62-67, vol.39, no.1, Jan. 1991.
- [19] R. A. Burberry, *VHF and UHF ANTENNAS*, Peter Peregrinus Ltd, London, 1992.
- [20] Sang-Wook Kim, Se-Yun Kim, and Sangwook Nam, "Estimation of the penetration angle of a man-made tunnel using time of arrival measured by short-pulse cross-borehole radar," *Geophysics*, 75, J11, 2010.
- [21] J. F. Vesecky, W. A. Nierenberg, and A. M. Despain, "Tunnel Detection," *SRI international*, Apr. 1980.

Publications

Conference papers

Dong-Hun Kim, Motoyuki Sato, Takatoshi Ito, “Dynamic Monitoring of Fracture Extension in Unconsolidated Sand Specimen by GPR,” *13th International Conference on Ground Penetrating Radar*, Lecce, Italy, June 22-25, 2010, pp. 828-833.

Dong-Hun Kim, Motoyuki Sato, “GPR Monitoring of Fracture Extension induced by hydraulic fracturing,” *2010 Asia-Pacific Radio Science Conference*, Toyama, Japan, Sep. 22-26, 2010, FP. 2.

Dong-Hun Kim, Motoyuki Sato, “Monitoring of water diffusion in the subsurface by cross-hole radar with an optical sensor array,” *123th Society of Exploration Geophysicists of Japan Conference*, Sendai, Japan, Sep. 29-Oct. 1, 2010, No. 29, pp. 107-110.

Dong-Hun Kim, Motoyuki Sato, “GPR monitoring of the fluid movement induced by hydraulic fracturing in unconsolidated sand,” *123th Society of Exploration Geophysicists of Japan Conference*, Sendai, Japan, Sep. 29-Oct. 1, 2010, No. 41, pp. 155-157.

Dong-Hun Kim, Motoyuki Sato, “GPR Monitoring of Fracture Extension induced by hydraulic fracturing,” *16th Formation Evaluation Symposium of Japan*, Chiba, Japan, Oct. 7-8, 2010, H.

Journal paper

“GPR Monitoring of Fracture Extension in Porous Material Induced by Hydraulic Fracturing” will be submitted to *Geophysics*.

Acknowledgement

I would like to thank Prof. Motoyuki Sato, Center for Northeast Asian Studies, Tohoku University, for providing me a chance of the research work and useful suggestions.

I would like to thank Prof. Takatoshi Ito, Institute of Fluid Science, Tohoku University, for giving me an instructive suggestion for the thesis construction.

I would like to thank Assoc. Prof. Yuichi Niibori, Graduate School of Engineering, Tohoku University, for giving me a correct suggestion for the thesis content.

I would like to thank laboratory members, Assistant Prof. Yuya Yokota, Dr. Jun Sonoda, Dr. Takashi Kido, Fumika Kawahara, Dr. Manabu Watanabe, Dr. Andrey Klovov, Dr. Naoki Hayashi, Dr. Jiong Chen, Khamis Kabeel, Masayoshi Matsumoto, Ahmed Gaber, Siwei Chen, Hai Liu, Shunichi Kusano, Riafeni Kalina, Naoki Muratani, Borol Erdenbat, Yong-Xi Zhang, Takafumi Kitajo and Naoko Makino. All of them make my academic life fun a lot.

During my stay in Sato laboratory, many people come and left. All of them gave me good advice and excitement. I also would like to thank them.

I would like to thank Dr. Kuroda, Laboratory of Engineering Geology, NIRE (National Institute for Rural Engineering), for cooperation borehole radar experiments.

I would like to thank Takayama, Toyota Industries Corporation, for cooperation hydraulic fracturing experiments.

I would like to thank KIST (Korea Institute of Science and Technology) IMRC (Imaging Media Research Center) members, Dr. Se-Yun Kim, Dr. Sang-Wook Kim, Dr. Seung-Yeup Hyun, Dr. Ji-Hyun Jung, Jea-Hyoung Cho. All of them help to enhance my engineering experience.

I would like to thank my parents and brother for exuberant support and love.